European Journal of Medicinal Chemistry 83 (2014) 1–14

Contents lists available at ScienceDirect

European Journal of Medicinal Chemistry

journal homepage: http://www.elsevier.com/locate/ejmech

Original article

Optimization of peptidomimetic boronates bearing a P3 bicyclic scaffold as proteasome inhibitors

Valeria Troiano [a], Kety Scarbaci [a], Roberta Ettari [b, *], Nicola Micale [a], Carmen Cerchia [c], Andrea Pinto [b], Tanja Schirmeister [d], Ettore Novellino [c], Silvana Grasso [e], Antonio Lavecchia [c, **], Maria Zappalà [a]

[a] Dipartimento di Scienze del Farmaco e dei Prodotti per la Salute, Università degli Studi di Messina, Viale Annunziata, 98168 Messina, Italy
[b] Dipartimento di Scienze Farmaceutiche, Università degli Studi di Milano, Via Mangiagalli 25, 20133 Milano, Italy
[c] Dipartimento di Farmacia, "Drug Discovery" Laboratory, Università degli Studi di Napoli Federico II, Via Domenico Montesano 49, 80131 Napoli, Italy
[d] Institute of Pharmacy and Biochemistry, University of Mainz, Staudinger Weg 5, D-55099 Mainz, Germany
[e] Dipartimento di Scienze Chimiche, Università degli Studi di Messina, Via F. Stagno D'Alcontres 31, 98166 Messina, Italy

ARTICLE INFO

Article history:
Received 26 March 2014
Received in revised form
5 June 2014
Accepted 9 June 2014
Available online 10 June 2014

Keywords:
Peptidomimetic boronates
Proteasome inhibitors
Docking studies

ABSTRACT

A new series of pseudopeptide boronate proteasome inhibitors (**2**–**3**) was developed, through optimization of our previously described analogs of bortezomib, bearing a bicyclic 1,6-naphthyridin-5(6*H*)-one scaffold as P3 fragment (**1**). The biological evaluation on human 20S proteasome displayed a promising inhibition profile, especially for compounds bearing a P2 ethylene fragment, which exhibited K_i values in the nanomolar range for the ChT-L activity (e.g. **2a**, K_i = 0.057 μM) and considerable selectivity for proteasome over bovine pancreatic α-chymotrypsin. Docking experiments into the yeast 20S proteasome revealed that the ligands are accommodated predominantly into the ChT-L site and that they covalently bind to the active site threonine residue via boron atom. Within the cellular assays performed against a 60 cancer cell line panel, compounds **3e** and **3f** demonstrated also good antiproliferative activity and compound **3f** emerged as promising lead compound for the development of anticancer agents targeting melanoma and non-small cell lung cancer.

1. Introduction

The 26S proteasome is the most important non-lysosomal, proteolytic complex, structurally composed by a central particle called 20S core, which exerts the catalytic activity, and two regulatory particles named 19S, which are located at both the ends of the catalytic core. The latter is made by four stacked rings, each one composed of seven different subunits. In detail, the two outer rings contain only α subunits and exert structural functions, whereas the two inner rings consist of β subunits and carry out the proteolytic activity [1].

Proteasome presents three different catalytic subunits which are classified on the basis of the amino acid after which they cleave the peptide bond: β1 or post-glutamyl peptidyl hydrolase (PGPH), recently more correctly referred to as caspase-like (C-L) site, which cleaves mainly after acidic amino acids; β2 or trypsin-like (T-L), that cleaves after basic amino acids; β5 or chymotrypsin-like (ChT-L) that cleaves after hydrophobic residues [2]. In all the catalytic subunits, the active site is represented by the N-terminal Thr, whose side chain hydroxyl group performs the nucleophilic attack onto the carbonyl carbon of the peptide bond [3].

Proteasome plays a fundamental role in the protein turnover by degrading misfolded, abnormal or damaged proteins, previously labeled through addition of a polyubiquitin chain. Most of proteasome substrates are involved in cell cycle regulation, angiogenesis and apoptosis, therefore defects of this system can lead to an anarchic cell proliferation [4]. As a consequence, proteasome inhibition has been identified as a promising strategy for anticancer therapy and the great efforts over the past decades led to the introduction in therapy of bortezomib (Velcade®, Fig. 1), the first proteasome inhibitor approved by FDA for the treatment of

Abbreviations: ChT-L, chymotrypsin-like; T-L, trypsin-like; PGPH, post-glutamyl peptide hydrolyzing; C-L, caspase-like; DMSO, dimethyl sulfoxide; EDC, 1-ethyl-3-(3-dimethylaminopropyl)carbodiimide; HOBt, *N*-hydroxybenzotriazole; DIPEA, N,N-diisopropylethylamine.

* Corresponding author.
** Corresponding author.
E-mail addresses: roberta.ettari@unimi.it (R. Ettari), antonio.lavecchia@unina.it (A. Lavecchia).

http://dx.doi.org/10.1016/j.ejmech.2014.06.017
0223-5234/

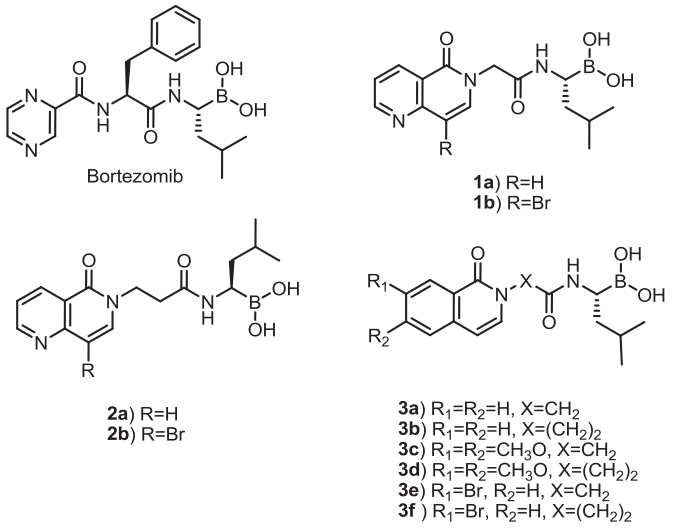

Fig. 1. Structures of bortezomib and compounds **1**–**3**.

relapsed and/or refractory multiple myeloma [5] and mantle cell lymphoma [6].

Although bortezomib has brought many benefits in patients with MM, its clinical use has been limited by its toxic side effects [5], the most serious of which include peripheral neuropathy and hematological toxicity. Considering all these problems, the development of peptidomimetics could lead to many pharmacokinetic and pharmacodynamic advantages. This strategy can be realized, for example, by introducing into a peptide framework unnatural amino acids instead of natural residues, or with the introduction of a non-peptidic scaffold into the peptidic backbone, in order to lock a defined conformation of the peptide [7–9].

Our research group has been involved in the recent past in the development of peptidomimetic 20S proteasome inhibitors [10], in this context, we recently described the synthesis of conformationally constrained pseudopeptide boronates [11], structurally related to bortezomib, bearing a 1,6-naphthyridin-5(6*H*)-one scaffold (e.g. **1a**–**b**, Fig. 1), which exhibited a promising profile of both activity and selectivity.

The N-1 atom of the naphthyridinone scaffold was assumed to reproduce the additional H-bond interaction of N-4 atom of bortezomib pyrazinamide with the side chain hydroxyl group of Asp114, located into the β6 subunit [12]. A docking experiment performed on the most potent compound of this series (**1b**) within the β5 binding site, showed that the inhibitor adopted a folded conformation stabilized by an intramolecular H-bond between the naphthyridinone carbonyl group and one of the hydroxyl moieties of the boronic acid warhead. As a consequence, the P3 naphthyridinone scaffold pointed towards the S2 pocket instead of the originally assumed S3 pocket [11].

On the basis of these findings, we replaced the P2 methylene fragment of the most active compounds (**1a**–**b**) with the ethylene homolog (**2a**–**b**, Fig. 1), assuming that the elongation of the central aliphatic chain should avoid the intramolecular H-bonding, by increasing the distance between the involved groups. This should induce a more similar conformation to that of bortezomib and improve the inhibition efficacy against the ChT-L activity. Our choice of the ethylene chain is justified also by its wide use in the field of peptidomimetics as β-alanine mimetic, since literature data indicate that the replacement of α-amino acids with β-ones allows to an increase the inhibition activity [13]. Furthermore, we developed a panel of inhibitors (**3a-f**) by replacing the naphthyridinone scaffold with the isoquinolin-1(2*H*)-one isostere, that lacks the N-1 atom, with the aim to evaluate its real contribution to the inhibitory activity. The P1 Leu-boronic moiety was not modified since it is essential to reversibly interact with the γ-OH group of N-terminal Thr of 20S proteasome. In this regard, while irreversible blockage of an enzyme is desirable for parasitic targets [14], on the contrary in the case of inhibition of endogenous proteases for cancer treatment, reversible or non-covalent inhibition would be advantageous.

Furthermore, the covalent binding mode of the designed inhibitors was clarified by performing docking analysis using the crystal structure of the yeast 20S proteasome. Moreover, growth inhibitory effects were evaluated at the National Cancer Institute (NCI) against sixty human tumor cell lines.

2. Results and discussion

2.1. Chemistry

Synthesis of the boronic acids **2a**–**b** and **3a**–**f** was performed as outlined in Scheme 1. Ester intermediates **5a**–**h** were synthesized through N-alkylation of the proper bicyclic scaffolds (**4a**–**e**) with ethyl 2-bromoacetate or methyl 3-bromopropionate, in the presence of NaH or KH. The subsequent alkaline hydrolysis gave the corresponding carboxylic acids **6a**–**h** which were coupled to pinanediol leucine boronate [15] **7** in the presence of HOBt, EDCI and DIPEA, to provide the pinanediol esters **8a**–**h**. In this step the corresponding amides **9** were also isolated as by-products. Finally, the pinanediol intermediates underwent a trans-esterification reaction with isobutylboronic acid under acidic conditions, to afford the peptide boronates **2**–**3**.

2.2. Inhibitory effect on the ChT-L, T-L and PGPH activities of human 20S proteasome

The inhibitory profile of peptidomimetic boronates **2**–**3** was evaluated on purified 20S proteasome isolated from human erythrocytes, using the appropriate fluorogenic substrate for each one of the proteolytic activities (i.e. Suc–Leu–Leu–Val–Tyr–AMC for ChT-L; Boc–Leu–Arg–Arg–AMC for T-L; Z-Leu–Leu–Glu–AMC for PGPH) and employing bortezomib as reference compound.

Compounds **2**–**3** underwent a preliminary screening for ChT-L activity at 20 μM, using an equivalent volume of dimethyl sulfoxide (DMSO) as a negative control. Since all compounds inhibited more than 40% of the enzyme activity, continuous assays were then performed at seven different concentrations using the progress curve method to determine the K_i values (Table 1).

Consistently with our initial hypothesis, almost all compounds bearing the ethylene chain as P2 fragment exhibited the highest inhibition potency against the ChT-L activity, with K_i values in the nanomolar range (**2a**, **3b**, **3d, 3f**). On the other hand, the analogs with a methylene P2 fragment demonstrated to be much less active (submicromolar/micromolar K_i values) or completely inactive, with the exception of compound **3e** ($K_i = 0.053$ μM). We may suppose that this result is due to a positive contribution of the bromine atom to enzyme inhibition, whereas, the introduction of the two methoxy groups (i.e. **3c**) resulted to hinder the inhibitory activity. Unexpectedly, no inhibition was recorded for compound **2b**.

All compounds inhibited the PGPH activity in a lesser extent compared to the ChT-L one, whereas no inhibition was shown against T-L activity. This outcome is particularly significant since literature data indicate that the suitable inhibition profile to optimize anticancer efficacy is the co-inhibition of the ChT-L activity together with either the PGPH or T-L ones [16], whereas the inhibition of the sole ChT-L activity produces only moderate effects [17], while the inhibition of all the activities results to be cytotoxic [18].

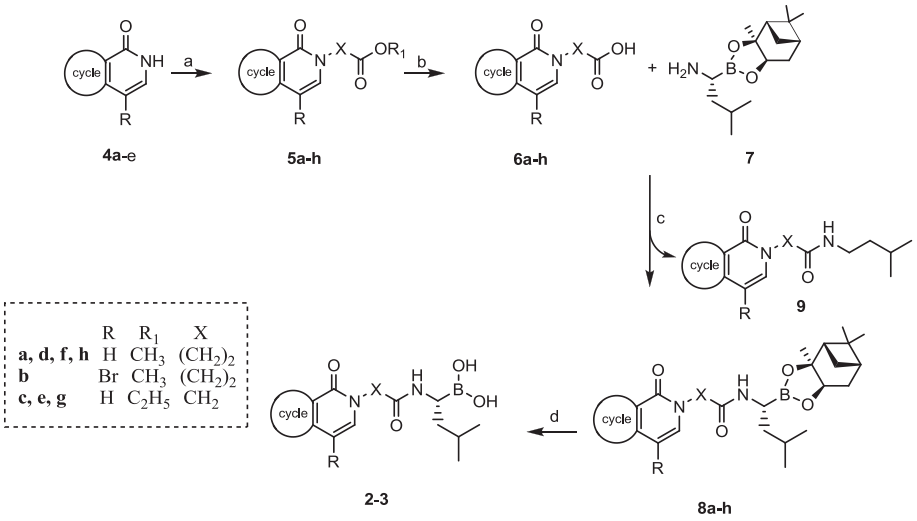

Cycle			
4a-b, **5a-b**, **6a-b**, **8a-b**, **9a-b**	**4c**, **5c-d**, **6c-d**, **8c-d**, **9c-d**	**4d**, **5e-f**, **6e-f**, **8e-f**, **9e-f**	**4e**, **5g-h**, **6g-h**, **8g-h**, **9g-h**

Scheme 1. Reagents and conditions: (a) NaH or KH, DMF, 0 °C, 1 h, then ethyl 2-bromoacetate or methyl 3-bromopropionate, rt or 50 °C, N_2, 2 h, 30–83%; (b) 1 N LiOH, EtOH or MeOH, 0 °C→rt, 6 h, 70–97%; (c) HOBt, CH_2Cl_2, −5 °C, 20 min, then EDC·HCl, DIPEA, **7**, −15 °C→rt, 3 h, 56–90%; (d) $iBuB(OH)_2$, 1 N HCl, MeOH/n-hexane (1:1), rt, 18 h, 28–36%.

The selectivity of compounds **2**–**3** towards the target protease was assessed by evaluating the inhibitory activity against bovine pancreatic α-chymotrypsin. All the inhibitors showed remarkable selectivity since they were demonstrated to be inactive or, in some cases, one/two orders of magnitude less active on the pancreatic protease if compared to 20S proteasome (Table 1).

Also the biological activity of the newly identified amides **9** was evaluated (Table 2), since we recently demonstrated [19] that some structurally-related amides showed to non-covalently

Table 1
Inhibition of ChT-L and PGPH activities of proteasome and pancreas bovine α-ChT by compounds **1**–**3**.

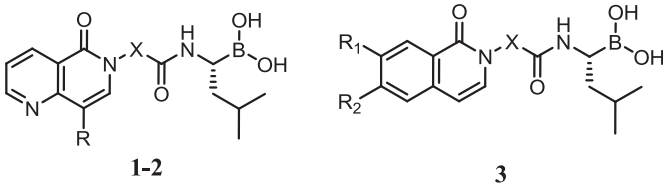

	X	*R*	R_1	R_2	ChT-L K_i (μM)[a]	PGPH K_i (μM)[a]	α-ChT K_i (μM)[a]
1a[b]	CH_2	H	–	–	0.44 ± 0.21	1.55 ± 0.41	n.i.
1b[b]	CH_2	Br	–	–	0.17 ± 0.01	17.6 ± 0.8	n.i.
2a	$(CH_2)_2$	H	–	–	0.057 ± 0.036	0.69 ± 0.38	n.i.
2b	$(CH_2)_2$	Br	–	–	n.i.	n.i.	n.i.
3a	CH_2	–	H	H	0.49 ± 0.11	0.99 ± 0.36	9.11 ± 1.77
3b	$(CH_2)_2$	–	H	H	0.051 ± 0.010	0.24 ± 0.03	n.i.
3c	CH_2	–	CH_3O	CH_3O	n.i.	n.i.	n.i.
3d	$(CH_2)_2$	–	CH_3O	CH_3O	0.085 ± 0.013	1.25 ± 0.03	n.i.
3e	CH_2	–	Br	H	0.053 ± 0.001	0.31 ± 0.02	0.29 ± 0.14
3f	$(CH_2)_2$	–	Br	H	0.06 ± 0.01	2.04 ± 0.64	23.7 ± 0.1
Bortezomib					9.8 nM		2.40 ± 0.20

[a] Values represent the mean of three independent determinations. n.i. = no inhibition.
[b] Data from ref. [9].

Table 2
Inhibition of ChT-L and PGPH activities of proteasome and pancreas bovine α-ChT by compounds **9a**–**b**, **g**.

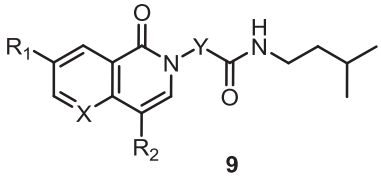

9

	X	Y	R_1	R_2	ChT-L K_i (μM)[a]	PGPH K_i (μM)[a]	α-ChT K_i (μM)[a]
9a	N	$(CH_2)_2$	H	H	4.57 ± 0.01	n.i.	n.d.
9b	N	$(CH_2)_2$	H	Br	0.08 ± 0.02	44% at 20 μM	n.i.
9g	CH	CH_2	Br	H	2.34 ± 0.61	n.i.	n.i.

n.i. = no inhibition; n.d. = not determined.
[a] Values represent the mean of three independent determinations.

inhibit the ChT-L activity. Amides **9a**, **9b** and **9g** were selected for continuous assays at seven different concentrations (Table 2). Amide **9b** emerged as the most active against the ChT-L activity with a K_i value of 80 nM, and a considerably lower activity against the PGPH one. No inhibition was recorded against the T-L activity.

2.3. Docking studies

To rationalize the SAR data and elucidate the molecular mechanism of proteasome inhibition of the described pseudo-peptide boronates, we planned to perform docking experiments of the inhibitors **2a**–**2b, 3a**–**3f** and **9b** into the binding pocket of the β5 subunit of the crystal structure of bortezomib in complex with the yeast 20S proteasome (PDB ID: 2F16) [12], following the protocol described in our recent papers [11,20]. Compounds **2a**, **3b**, **3d** and **3f**, which have a more flexible P2 ethylene fragment, were proven to bind in an identical mode to the ChT-L site, which explains their similar K_i values. As depicted in Fig. 2, the inhibitors were found to adopt a β-conformation and to fill the gap between strands S2 and S4 by forming H-bonds with residues T21, G47, and A49 of β5 subunit. This binding mode elucidates the high affinity of these compounds to the ChT-L active site. The P1-leucine side chain of all inhibitors was found to project into the S1 pocket adopting the same spatial arrangement of the corresponding moiety of bortezomib. K33, M45, A49 and V31 of subunit β5 stabilized the P1 leucine side chain through van der Waals

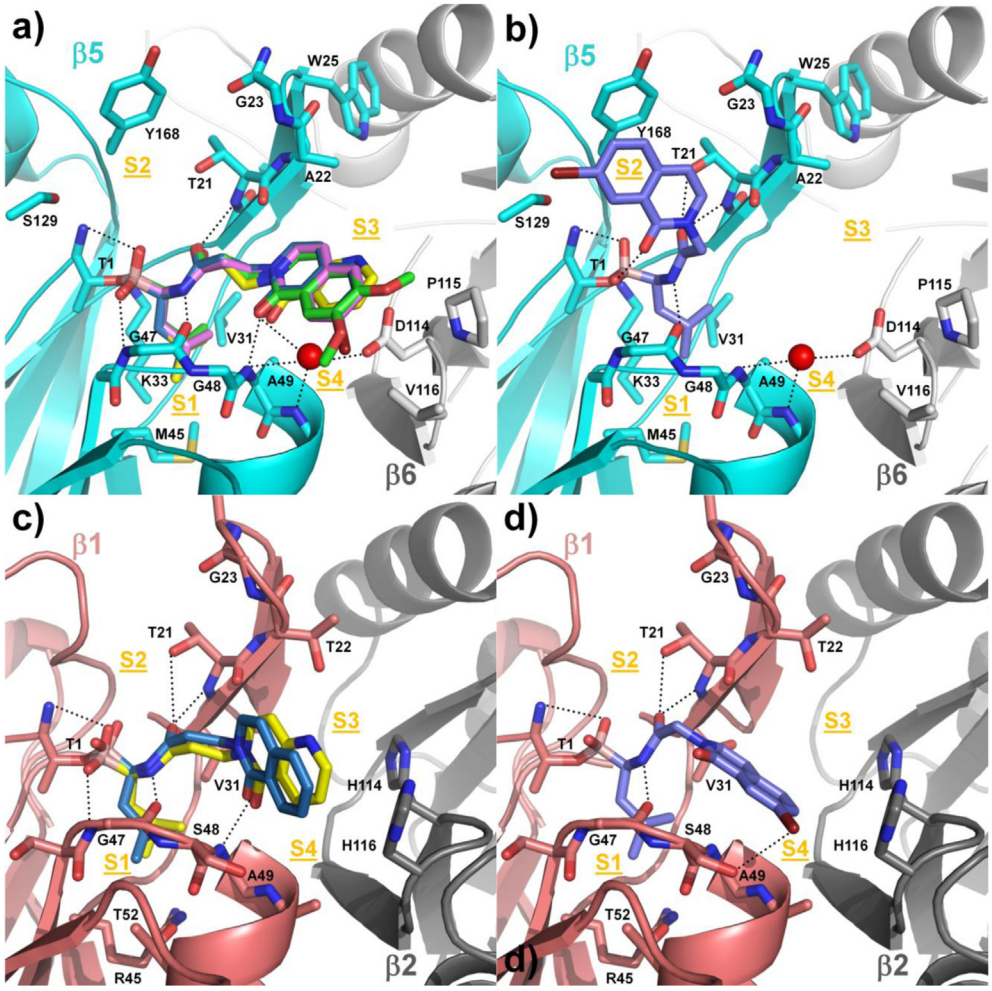

Fig. 2. Binding modes of inhibitors into the yeast 20S proteasome. (a) Structural superposition of the compounds **2a** (yellow), **3b** (skyblue), **3d** (green), and **3f** (magenta) bound to the ChT-L active site. (b) Binding mode of compound **3e** (purple) into the ChT-L active site. Subunits β5 (cyan) and β6 (gray) are both shown in cartoon representations. (c,d) Binding mode of compounds **2a** (yellow), **3b** (skyblue) and **3e** (purple) into the C-L active site. Subunits β1 (deepsalmon) and β2 (black) are both shown in cartoon representations. Only amino acids located within 4 Å of the bound ligand are displayed and labeled. Key H-bonds between the inhibitors and the protein are shown as dashed black lines. The defined water molecule forming tight H-bonds to the protein is displayed as a red sphere. S1–S4 pockets of the proteasome are labeled. (For interpretation of the references to color in this figure legend, the reader is referred to the web version of this article.)

interactions. The large naphthyridinone moiety of **2a** and the isoquinolinone moiety of **3b**, **3d** and **3f** protruded into the spacious S4 pocket located in β6 subunit, and formed van der Waals interactions with P115 and V116, thereby stabilizing these moieties in the ChT-L site.

Moreover, the pyridone C]O oxygen of ligands established H-bonds with β5-A49N, β5-A50N and β6-D114O$^{\gamma}$ via an intervening water molecule located crystallographically in the bortezomib structure [12] and included in our model. This indirect water-mediated H-bond to β6-Asp114, a crucial residue to retain the ChT-L inhibitory activity, provides an explanation for the selective inhibition of these inhibitors against the ChT-L activity of proteasome.

The inactivity of compound **2b** can be attributed both to the bromine withdrawing effect, which weakens the H-bonding capability of the pyridone C]O oxygen, and to a steric clash between the bulky bromine atom on the naphthyridinone moiety and the Ala22 residue in the β5 subunit, which leads to a repositioning of the entire molecule in the ChT-L binding pocket. A comparison of the binding mode of compound **2b** and its corresponding by-product **9b**, which is the most active inhibitor of ChT-L site among amides, reveals that the 3-(8-bromo-5-oxo-1,6-naphthyridin-6(5H)-yl)-N-isopentylpropanamide scaffold, common to both ligands, occupies different positions in the binding cavity. Therefore, there is no relationship between the effect of bromine atom in compound **2b** and that in compound **9b**. Unlike **2b**, which is a boron-containing compound, **9b** is a noncovalent inhibitor which inhibits the proteasome through a different binding mode, stabilized by a network of interactions (hydrophobic, hydrogen bonds, electrostatic, and/or van der Waals) with specific residues of the ChT-L active site. The binding mode of a compound similar to amide **9b** has been described in our recent publication [19].

When compounds **3a**, **3c**, and **3e**, which have a less flexible P2 methylene fragment, were docked within the β5 subunit binding pocket, a folded conformation, stabilized by an intramolecular H-bond between the pyridone C]O oxygen and one of the OH groups of the boronic acid fragment, was largely found. Fig. 2b shows the binding mode of the representative compound **3e** into the ChT-L active site. This result is coincident with that previously described for compounds **1a** and **1b** [11]. In this binding conformation, the ligand backbone was stabilized by H-bonds with β5-G47N, β5-T21N and β5-T21O$^{\gamma}$, whereas the isoquinolinone moiety protruded into the S2 specificity pocket, a rather large and solvent exposed cavity able to accept space-demanding substituents. The benzo-fused aromatic ring of **3a** appeared to be optimally oriented for a favorable face-on-face π–π stacking interaction with β5-Y168. Interestingly, the incorporation of an electron-withdrawing bromine group, as in **3e**, enhanced the observed ChT-L inhibitory activity ($K_i = 0.05$ μM) due to electronic effects associated with a more favorable π-stacking [21] of the inhibitor above the electron rich β5-Y168. On the other hand, the poor inhibitory activity of **3c**, which holds two methoxy groups on the isoquinolinone ring, is not only due to steric hindrance of the methoxy groups with β5-Y168 side chain but also to an unfavorable electron-donating effect of the substituents, which donate excess electrons into the π-system and decrease the π–π stacking interaction with β5-Y168.

Although compounds **2a**, **3b** and **3e** preferentially targeted the β5 active site, they also showed, in a lesser extent, PGPH inhibitory activity (see Table 1). To elucidate the structural determinants underlying the lack of selectivity towards the proteasomal subsite of these compounds, we carried out docking experiments into the β1 active site using the bortezomib/20S proteasome crystal structure. Docking results showed that **2a**, **3b** and **3e** adopted a binding mode similar to that crystallographically observed for bortezomib, filling the gap between strands S2 and S4. Main chain atoms of the ligands formed H-bonds with the conserved residues β1-G47O, β1-T21N and β1-T21O. The P1 leucine side chain of all the three compounds protruded into the S1 pocket of the C-L site that, differently from the ChT-L site, is highly polar, thus providing an explanation to the lower compound affinity observed towards this active site. The P3 group has a major effect on the binding profile. Unlike bortezomib, that directs its pyrazine nucleus towards the S3 pocket creating a key interaction with β1-T22O$^{\gamma}$ residue, the bicyclic aromatic scaffold of inhibitors sat nicely in the S4 binding pocket, forming specific interactions (Fig. 2c). In particular, the pyridinone C]O oxygens of **2a** and **3b** established an H-bond with β1-A49N, whereas the benzo- and pyrido-fused rings formed an edge-to-face π-stacking interaction with the imidazole ring of H116 of the adjacent β2 subunit. In contrast, the substituted isoquinolinone moiety of **3e** adopted a slightly different orientation within the S4 pocket (Fig. 2d) due to the formation of a halogen bond between the bromine atom and the oxygen atom of the β1-S48 side chain. It should be noted that compound **3e** assumes surprisingly an extended conformation moving from the ChT-L site to the C-L site. A possible explanation for this behavior is that in ChT-L site the ligand is forced to assume a folded conformation to form a tight π–π stacking interaction with β5-Y168, which in the C-L site cannot be formed because Y168 is replaced by S168. On the contrary, in the C-L site, the ligand preferably adopts an extended conformation to engage in a favorable halogen bond with β1-S48, which cannot be formed in the ChT-L site because S48 is replaced by G48. Therefore, the lack of specificity of **2a** and **3b** is probably a consequence of a common binding pattern of the P3 moiety in both ChT-L and C-L site. In particular, the H-bonding with D114 that stabilizes the P3 site of the ligands in the ChT-L site cannot be formed in the C-L site due to the presence of a histidine residue at the position 114 of the neighboring subunit β2. However, the bicyclic aromatic scaffold is stabilized by other residues, including β2-His116, which are specific for C-L site. The unspecific binding of **3e** is instead due to its ability to adopt a folded or extended binding conformation forming interactions with specific residues of both ChT-L (β5-Y168) and C-L (β1-S48) subunits of the 20S proteasome.

2.4. Anticancer activity assay

Compounds **2**–**3** and **9** were submitted to NCI to test their cytotoxic and/or growth inhibitory effects. Ten compounds (**2a**, **3a**–**f**, **9c**, **9f**, **9h**) were selected for the preliminary screening at 10 μM, against 60 tumor cell lines representing Leukemia (L, 5 cell lines), Melanoma (M, 9 cell lines), Non-Small Cell Lung Cancer (NSCLC, 8 cell lines), Colon Cancer (CC, 7 cell lines), Central Nervous System Cancer (CNSC, 6 cell lines), Ovarian Cancer (OC, 7 cell lines), Renal Cancer (RC, 8 cell lines), Prostate Cancer (PC, 2 cell lines) and Breast Cancer (BC, 6 cell lines). The results are reported in Table 3 as mean percent growth values of each subpanel. Overall, amides **9** did not show any antiproliferative effects, demonstrating sometimes even a slight ability to stimulate cell growth. Only compound **9h** displayed poor cell growth inhibition properties against a panel of L cells (mean% growth = 83.4%) and RC one (mean% growth = 86.1%).

Concerning boronates, the preliminary screening showed promising activity for compounds **3e**–**f**, which showed higher efficacy against the cell lines belonging to L, M, RC and BC panels, and for compound **2a**, which was proven to be active against L cell lines. In particular, inhibitors **3e**–**f** exhibited remarkable ability to inhibit cancer cell proliferation leading to residual percent growth, sometimes nearly to zero (e.g. 0.02% and 0.6% growth of L cell lines for compounds **3f** and **3e**, respectively).

Table 3
Anticancer activity of compounds **2a**, **3a**–**f**, **9c**, **f**–**h** as mean % growth at 10 μM.

Panel	2a	3a	3b	3c	3d	3e	3f	9c	9f	9h
L	34.76	23.13	21.15	98.75	59.03	0.57	0.02	99.55	107.62	83.42
NSCLC	80.27	75.56	60.34	101.52	90.27	22.00	8.79	97.17	99.21	97.74
CC	78.09	57.93	45.10	104.46	90.85	3.27	4.45	100.50	105.72	103.83
CNSC	82.86	71.03	51.95	99.62	78.28	24.29	6.51	102.36	98.00	97.25
M	60.42	43.50	30.53	103.95	63.71	−17.12	−19.16	103.50	105.84	93.97
OC	84.19	86.69	73.14	102.52	92.58	37.47	38.80	104.22	103.14	104.41
RC	76.14	39.82	32.27	98.47	88.98	−8.89	−4.00	97.42	95.30	86.13
PC	98.52	80.20	57.81	100.06	98.78	42.89	34.47	101.12	102.64	103.37
BC	68.02	51.30	38.09	99.03	56.94	2.23	2.31	102.69	102.96	94.48

In some cases, they showed to generate cytotoxic effects in the tested tumor cell lines as it is outlined by the negative percent growth values recorded, which indicate a decrease of the cell population compared to that of time zero (Tz, time of drug addition). This result is particularly important since cytotoxicity is a desirable effect within the antitumor therapy.

Compounds **2a**, **3b**, **3e** and **3f** were selected for further evaluation within the five dose screening, ranging from 100 μM to 0.01 μM, against a panel of 60 human cancer cell lines. The antitumor activity of the tested compounds (Tables 4 and 5) is expressed by three different dose–response parameters: GI_{50} (concentration required to reduce cell growth to 50%), TGI (concentration leading to total growth inhibition) and LC_{50} (concentration required for 50% cell death).

Compound **2a** (Table 4) showed GI_{50} values at micromolar level, ranging from 2.04 μM to 60.2 μM. It exhibited the highest growth inhibition potency against the following cancer cell lines: MDA-MB-468 (BC, GI_{50} = 2.04 μM), CCRF-CEM (L, GI_{50} = 2.35 μM), MDA-MB-435 (M, GI_{50} = 2.41 μM), NCI-H226 (NSCLC, GI_{50} = 2.68 μM) and SF-539 (CNSC, GI_{50} = 2.76 μM). Compound **2a** showed also TGI values at micromolar level, ranging from 7.02 μM to 71.3 μM and the best results were obtained against MDA-MB-435 (M, TGI = 7.02 μM), SF-539 (CNSC, TGI = 8.38 μM), NCI-H226 (NSCLC, TGI = 8.90 μM), and MDA-MB-468 (BC, TGI = 9.96 μM). Furthermore, this compound exhibited some cytotoxic properties, in particular against NCI-H226 (NSCLC, LC_{50} = 48.0 μM) and RXF 393 (RC, LC_{50} = 54.2 μM).

Compound **3b** (Table 4) showed GI_{50} values in the micromolar range, from 1.06 μM to 76.8 μM. It showed the highest growth inhibition activity against the following cancer cell lines: RPMI-8226 (L, GI_{50} = 1.06 μM), A498 (RC, GI_{50} = 1.22 μM), MDA-MB-435 (M, GI_{50} = 1.27 μM) and MOLT-4 (L, GI_{50} = 1.28 μM). Also in the case of TGI micromolar values were recorded and the best results were achieved against the melanoma cancer cell line MDA-MB-435 (TGI = 2.81 μM) and the non-small cell lung cancer cell line NCI-H226 (TGI = 3.24 μM). Against the same cell lines, compound **3b** exhibited also a satisfactory cytotoxicity profile (NCI-H226, LC_{50} = 7.15 μM and MDA-MB-435, LC_{50} = 6.24 μM).

Compound **3e** (Table 5) demonstrated a remarkable antiproliferative activity with GI_{50} values ranging from 0.10 μM to 6.31 μM. It was proven to be active at low submicromolar concentrations against many cancer cell lines [e.g. A498 (RC, GI_{50} = 0.10 μM), SR (L, GI_{50} = 0.27 μM), MDA-MB-468 (BC, GI_{50} = 0.30 μM)]. Against A498 cell line, inhibitor **3e** exhibited also a remarkable TGI value = 0.58 μM, whereas for most of the other cell lines it exhibited TGI values in the micromolar range (TGI = 1.10–75.1 μM). Compound **3e** demonstrated also good cytotoxic effects exhibiting LC_{50} values that in some cases reached the low micromolar level [i.e. NCI-H226 (NSCLC, LC_{50} = 5.39 μM), MDA-MB-435 (M, LC_{50} = 5.88 μM), RXF 393 (RC, LC_{50} = 5.99 μM), LOX IMVI (M, LC_{50} = 7.21 μM), SK-MEL5 (M, LC_{50} = 7.88 μM), NCI-H522 (NSCLC, LC_{50} = 9.06 μM)].

Lastly, compound **3f** (GI_{50} = 0.13–17.4 μM, Table 5) demonstrated a remarkable antiproliferative activity since it was active at submicromolar level against most of the tested cancer cell lines. M (GI_{50} = 0.18–0.73 μM), RC (GI_{50} = 0.13–1.50 μM), L (GI_{50} = 0.26–1.08 μM), CNSC (GI_{50} = 0.21–1.18 μM), and BC (GI_{50} = 0.26–1.20 μM) cell panels resulted to be the most sensitive. Among these cell panels, compound **3f** inhibited cell growth at low submicromolar level in the following cancer cell lines: A498 (RC, GI_{50} = 0.13 μM), MDA-MB-435 (M, GI_{50} = 0.18 μM), SF-539 (CNSC, GI_{50} = 0.21 μM), LOX IMVI (M, GI_{50} = 0.22 μM), MDA-MB-468 (BC, GI_{50} = 0.26 μM), SR (L, GI_{50} = 0.26 μM) and RXF 393 (RC, GI_{50} = 0.28 μM). Furthermore, it showed submicromolar values against NCI-H226 (NSCLC, GI_{50} = 0.19 μM) and PC DU-145 (GI_{50} = 0.71 μM) cell lines, the latter being so much affected by any of the previously discussed compounds (i.e. **2a**, **3b** and **3e**). Remarkably, compound **3f** exhibited also submicromolar TGI values against MDA-MB-435 (M, TGI = 0.37 μM), NCI-H226 (NSCLC, TGI = 0.42 μM), SF-539 (CNS, TGI = 0.60 μM), LOX IMVI (M, TGI = 0.61 μM), A498 (RC, TGI = 0.74 μM), MDA-MB-468 (BC, TGI = 0.74 μM) and RXF 393 (RC, TGI = 0.88 μM). Concerning LC_{50} values, compound **3f** gave the best results against MDA-MB-435 (M, LC_{50} = 0.78 μM) and NCI-H226 (NSCLC, LC_{50} = 0.95 μM). Overall, NCI-H226 and MDA-MB-435 cell lines emerged as the best targets for compound **3f** due to their TGI, GI_{50} and LC_{50} values composition.

3. Conclusions

In conclusion, we developed a panel of conformationally constrained pseudopeptide boronates with high target-selectivity and an optimal inhibition profile, since they inhibit two of the three proteolytic subunits of 20S proteasome and they show remarkable selectivity towards the ChT-L one. Consistently to our hypothesis, we identified the ethylene chain as a suitable P2 fragment to increase the inhibition potency against the ChT-L activity, as it represents the common structural feature of all the most potent compounds of this series (**2a**, **3b**,**d**,**f**), which showed K_i values in the nanomolar range.

Finally, the replacement of naphthyridinone scaffold with the isoquinolinone isostere did not seem to influence the inhibitory activity profile, demonstrating no strict relationship between the presence of N-1 atom and the potency of the inhibitor. Compounds **3e** and **3f** demonstrated also good activity in antiproliferative assays showing low submicromolar GI_{50} values against most of the tested tumor cell lines. Furthermore, compound **3f** exhibited promising cytotoxic properties against the melanoma MDA-MB-435 and the non-small cell lung cancer NCI H226 cell lines, opening the way to further optimizations, with the aim to more effectively act on these kinds of malignancy. Docking experiments into the yeast 20S proteasome revealed their covalent binding mode and will allow future optimization of this interesting class of inhibitors.

Table 4
In vitro anticancer activity of compounds **2a**, **3b** and bortezomib against 60 human cancer cell lines.

Panel/Cell line	**2a**			**3b**			Bortezomib
	GI_{50} (μM)	TGI (μM)	LC_{50} (μM)	GI_{50} (μM)	TGI (μM)	LC_{50} (μM)	GI_{50} (nM)
Leukemia							
CCRF-CEM	2.35	>100	>100	2.02	25.4	>100	0.35
HL-60(TB)	6.88	>100	–	2.69	49.5	>100	1.90
K-562	17.2	>100	>100	4.97	>100	>100	1.17
MOLT-4	3.30	>100	>100	1.28	5.94	>100	0.51
RPMI-8226	3.22	>100	>100	1.06	7.07	>100	0.23
SR	3.18	>100	>100	1.70	28.9	>100	0.85
Non-small cell lung cancer							
A549/ATCC	38.0	>100	>100	8.41	>100	>100	3.09
EKVX	–	–	–	–	–	–	3.02
HOP-62	29.8	>100	>100	4.51	22.1	96.4	4.47
HOP-92	16.8	71.3	>100	10.9	67.1	>100	1.00
NCI-H226	2.68	8.90	48.0	1.47	3.24	7.15	0.46
NCI-H23	25.4	>100	>100	25.4	>100	>100	1.00
NCI-H322M	>100	>100	>100	76.8	>100	>100	17.8
NCI-H460	36.2	>100	>100	13.0	56.2	>100	4.47
NCI-H522	4.66	21.7	>100	2.61	8.09	>100	1.44
Colon cancer							
COLO-205	10.0	>100	>100	5.06	>100	>100	1.23
HCC-2998	13.6	35.0	90.2	6.08	21.3	66.4	0.60
HCT-116	3.30	16.5	86.2	1.55	19.8	>100	0.60
HCT-15	21.3	>100	>100	9.57	>100	>100	1.51
HT29	6.77	>100	>100	3.68	48.7	>100	0.95
KM12	17.0	49.6	>100	7.51	29.8	>100	1.70
SW-620	4.62	>100	>100	3.00	12.0	93.4	0.55
Central nervous system cancer							
SF-268	14.7	>100	>100	5.69	30.4	>100	1.17
SF-295	8.92	36.0	>100	3.78	19.6	83.3	1.70
SF-539	2.76	8.38	>100	1.61	5.62	>100	0.59
SNB-19	41.2	>100	>100	8.02	>100	>100	2.04
SNB-75	13.3	44.9	>100	2.94	15.9	93.4	2.04
U251	33.0	>100	>100	4.23	>100	>100	1.55
Melanoma							
LOX IMVI	6.37	28.4	>100	2.11	6.78	>100	0.78
MALME-3M	5.12	62.2	>100	2.58	9.89	>100	0.45
M14	4.11	22.3	97.9	4.23	>100	>100	0.93
MDA-MB-435	2.41	7.02	67.8	1.27	2.81	6.24	0.44
SK-MEL-2	18.3	>100	>100	3.58	32.5	>100	1.07
SK-MEL-28	7.17	>100	>100	3.27	>100	>100	0.46
SK-MEL-5	4.03	22.1	>100	4.30	19.0	83.7	0.68
UACC-257	10.1	47.0	>100	3.68	33.8	>100	0.59
UACC-62	5.55	48.8	>100	4.29	24.9	>100	0.91
Ovarian cancer							
IGROV1	60.2	>100	>100	12.3	>100	>100	2.24
OVCAR-3	4.65	31.9	>100	1.97	5.66	31.7	0.54
OVCAR-4	28.4	>100	>100	17.0	>100	>100	1.95
OVCAR-5	17.1	>100	>100	18.8	>100	>100	1.55
OVCAR-8	37.5	>100	>100	15.3	>100	>100	2.63
NCI/ADR-RES	>100	>100	>100	67.1	>100	>100	12.3
SK-OV-3	>100	>100	>100	4.72	81.3	>100	13.8
Renal cancer							
786-0	7.94	>100	>100	4.76	>100	>100	1.44
A498	3.07	24.3	>100	1.22	4.79	>100	0.48
ACHN	9.15	>100	>100	1.75	>100	>100	0.79
CAKI-1	19.4	>100	>100	2.93	27.0	>100	0.66
RXF 393	3.29	14.3	54.2	–	–	–	0.71
SN12C	18.0	>100	>100	11.2	55.4	>100	1.10
TK-10	5.16	47.7	>100	2.93	9.80	>100	1.00
UO-31	19.4	>100	>100	3.92	35.3	>100	1.05
Prostate cancer							
PC-3	41.4	>100	>100	5.77	>100	>100	2.63
DU-145	32.7	>100	>100	9.13	>100	>100	1.70
Breast cancer							
MCF7	3.61	>100	>100	4.35	>100	>100	0.55
MDA-MB-231/ATCC	7.94	32.5	>100	9.45	59.3	>100	1.26
HS 578T	15.6	>100	>100	3.63	48.7	>100	1.02
BT-549	3.49	12.5	>100	2.21	17.1	>100	0.55
T-47D	4.67	>100	>100	3.71	29.3	>100	0.60
MDA-MB-468	2.04	9.96	>100	1.38	7.08	>100	1.48

Table 5
In vitro anticancer activity of compounds **3e** and **3f** against 60 human cancer cell lines.

Panel/cell line	**3e**			**3f**		
	GI_{50} (μM)	TGI (μM)	LC_{50} (μM)	GI_{50} (μM)	TGI (μM)	LC_{50} (μM)
Leukemia						
CCRF-CEM	0.44	>100	>100	0.43	>100	>100
HL-60(TB)	0.38	5.34	>100	–	–	>100
K-562	3.15	>100	>100	1.08	>100	>100
MOLT-4	0.30	1.57	>100	0.31	>100	>100
RPMI-8226	0.32	>100	>100	0.32	>100	>100
SR	0.27	12.2	>100	0.26	11.6	>100
Non-small cell lung cancer						
A549/ATCC	4.58	>100	>100	2.39	>100	>100
EKVX	–	–	–	–	–	–
HOP-62	4.94	27.6	>100	2.63	9.29	>100
HOP-92	2.56	8.70	>100	1.34	5.61	>100
NCI-H226	0.47	1.84	5.39	0.19	0.42	0.95
NCI-H23	5.05	>100	>100	1.59	>100	>100
NCI-H322M	>100	>100	>100	>100	>100	>100
NCI-H460	5.58	36.8	>100	3.18	>100	>100
NCI-H522	0.59	2.54	9.06	0.30	2.25	>100
Colon cancer						
COLO-205	2.83	>100	>100	0.85	>100	>100
HCC-2998	2.46	6.37	31.4	1.14	3.09	8.42
HCT-116	0.60	3.57	95.8	0.34	2.55	>100
HCT-15	3.04	>100	>100	1.61	22.1	>100
HT29	0.73	5.52	>100	0.45	>100	>100
KM12	3.55	17.3	>100	1.33	4.38	>100
SW-620	0.46	8.19	>100	0.38	>100	>100
Central nervous system cancer						
SF-268	3.76	31.9	>100	0.70	3.85	>100
SF-295	2.03	15.9	86.4	0.58	4.51	75.5
SF-539	–	–	–	0.21	0.60	>100
SNB-19	3.86	>100	>100	0.96	>100	>100
SNB-75	2.13	9.09	63.3	0.46	3.82	>100
U251	5.56	>100	>100	1.18	>100	>100
Melanoma						
LOX IMVI	0.43	1.85	7.21	0.22	0.61	–
MALME-3M	4.31	>100	>100	0.68	7.95	>100
M14	1.25	6.73	>100	0.36	3.88	>100
MDA-MB-435	0.33	1.29	5.88	0.18	0.37	0.78
SK-MEL-2	–	–	–	0.46	4.56	>100
SK-MEL-28	–	–	–	0.52	29.7	>100
SK-MEL-5	0.80	2.65	7.88	0.37	3.11	82.5
UACC-257	0.94	4.51	>100	0.73	2.86	–
UACC-62	1.86	10.4	97.0	0.46	2.44	28.5
Ovarian cancer						
IGROV1	6.16	46.9	>100	5.10	>100	>100
OVCAR-3	0.60	3.95	>100	0.33	1.21	10.6
OVCAR-4	4.94	>100	>100	2.06	>100	>100
OVCAR-5	–	–	–	3.15	97.3	>100
OVCAR-8	3.53	>100	>100	3.64	>100	>100
NCI/ADR-RES	21.5	>100	>100	17.4	>100	>100
SK-OV-3	8.73	>100	>100	2.36	71.5	>100
Renal cancer						
786-0	4.06	>100	>100	0.82	>100	>100
A498	0.10	0.58	28.6	0.13	0.74	>100
ACHN	–	–	–	0.41	>100	>100
CAKI-1	0.41	10.5	>100	0.47	10.0	>100
RXF 393	0.43	1.77	5.99	0.28	0.88	5.39
SN12C	3.52	55.2	>100	1.50	11.5	>100
TK-10	0.65	7.22	>100	0.37	15.6	>100
UO-31	1.61	11.1	61.6	0.98	15.4	>100
Prostate cancer						
PC-3	6.31	>100	>100	4.19	>100	>100
DU-145	6.05	>100	>100	0.71	>100	>100
Breast cancer						
MCF7	0.42	>100	>100	0.39	>100	>100
MDA-MB-231/ATCC	3.18	19.8	>100	1.20	12.2	>100
HS 578T	2.94	75.1	>100	0.43	6.20	>100
BT-549	0.44	2.65	>100	0.36	4.32	>100
T-47D	0.78	12.4	>100	0.78	6.09	>100
MDA-MB-468	0.30	1.10	>100	0.26	0.74	>100

4. Experimental protocols

4.1. Chemistry

All reagents and solvents were obtained from commercial suppliers and were used without further purification. Elemental analyses were carried out on a C. Erba Model 1106 (Elemental Analyzer for C, H and N) and the obtained results are within ±0.4% of the theoretical values. Merck Silica Gel 60 F_{254} plates were used as analytical TLC; flash column chromatography was performed on Merck Silica Gel (200–400 mesh). ^{1}H and ^{13}C NMR spectra were recorded on a Varian Gemini 300 MHz, Varian Gemini 500 MHz and Bruker 300 MHz spectrometers using the residual signal of the deuterated solvent as internal standard. Splitting patterns are described as singlet (s), doublet (d), doublet of doublet (dd), triplet (t), doublet of triplet (dt), quartet (q), multiplet (m) and broad singlet (bs). ^{1}H and ^{13}C chemical shifts are expressed in δ (ppm) and coupling constants (J) in hertz (Hz). MS analyses were performed on a Varian 320-MS triple quadrupole mass spectrometer equipped with an electron spray ionization (ESI) source.

4.1.1. Synthesis of pseudopeptide boronates ***2***–***3***

*4.1.1.1. 3-(5-Oxo-5H-1,6-naphthyridin-6-yl)propionic acid methyl ester (**5a**).* A suspension of commercially available 1,6-naphthyridin-5(6*H*)-one **4a** (188 mg, 1.29 mmol) and NaH (37 mg, 1.55 mmol) in dry DMF (10 mL) was left under stirring at 0 °C for 1 h. Then, a solution of methyl 3-bromopropionate (197 μL, 1.81 mmol) in dry DMF (3 mL) was added dropwise and the reaction mixture was stirred at 50 °C for 18 h. After quenching NaH with saturated NH_4Cl solution (5 mL), the reaction mixture was extracted with $CHCl_3$ (3× 15 mL) and the organic phase was washed first with saturated $NaHCO_3$ solution (2× 20 mL) and then with distilled water (2 × 20 mL). The organic layer was dried over Na_2SO_4 and filtered, and the solvent was removed in vacuo. The crude was purified by column chromatography ($CHCl_3$/MeOH = 95:5) to give the title compound **5a** as a white solid (183 mg, 61%); R_f = 0.48 ($CHCl_3$/MeOH 95:5). ^{1}H NMR (300 MHz, $CDCl_3$): δ 2.90 (t, 2H, J = 6.6 Hz), 3.68 (s, 3H), 4.28 (t, 2H, J = 6.6 Hz), 6.8 (d, 1H, J = 7.0 Hz), 7.4 (dd, 1H, J = 7.6 Hz), 7.5 (d, 1H, J = 7.0 Hz), 8.7 (d, 1H, J = 7.6 Hz), 8.90 (s, 1H).

*4.1.1.2. 3-(8-Bromo-5-oxo-5H-1,6-naphthyridin-6-yl)propionic acid methyl ester (**5b**).* Compound **5b** was obtained following the same procedure reported for compound **5a**, using 8-Bromo-1,6-naphthyridin-5(6*H*)-one [22] **4b** (190 mg, 0.84 mmol), methyl 3-bromopropionate (229 μL, 2.10 mmol) and NaH (24 mg, 1.01 mmol). Purification by column chromatography (EtOAc/light petroleum 8:2) yielded the title ester **5b** as a pale yellow solid (150 mg, 57%); R_f = 0.61 (EtOAc/light petroleum 8:2). ^{1}H NMR (300 MHz, $CDCl_3$): δ 2.92 (t, 2H, J = 6.2 Hz), 3.65 (s, 3H), 4.25 (t, 2H, J = 6.2 Hz), 7.48 (dd, 1H, J = 6.6, 3.1 Hz), 7.83 (s, 1H), 8.69 (d, 1H, J = 6.6 Hz), 9.04 (d, 1H, J = 3.1 Hz).

*4.1.1.3. (1-Oxo-1H-isoquinolin-2-yl)acetic acid ethyl ester (**5c**).* A suspension of commercially available isoquinolin-1(2*H*)-one **4c** (200 mg, 1.38 mmol) and NaH (40 mg, 1.66 mmol) in dry DMF (10 mL) was left under stirring at 0 °C for 1 h. Then, a solution of ethyl 2-bromoacetate (214 μL, 1.93 mmol) in dry DMF (3 mL) was added dropwise and the reaction mixture was stirred at room temperature for 2 h. Work-up was carried out in the same way as for compound **5a**. Purification by column chromatography (EtOAc/*n*-hexane 4:6) yielded the title ester **5c** as white crystals (220 mg, 69%); R_f = 0.43 (EtOAc/*n*-hexane 4:6). ^{1}H NMR (300 MHz, $CDCl_3$): δ 1.29 (t, 3H, J = 7.0 Hz), 4.25 (q, 2H, J = 7.0 Hz), 4.71 (s, 2H), 6.53 (d,

1H, $J = 7.3$ Hz), 7.01 (d, 1H, $J = 7.3$ Hz), 7.48–7.53 (m, 2H), 7.65 (t, 1H, $J = 7.0$ Hz), 8.42 (d, 1H, $J = 8.1$ Hz).

*4.1.1.4. 3-(1-Oxo-1H-isoquinolin-2-yl)propionic acid methyl ester (**5d**).* Compound **5d** was obtained following the same procedure reported for compound **5a**, using **4c** (200 mg, 1.38 mmol), methyl 3-bromopropionate (376 μL, 3.45 mmol) and NaH (40 mg, 1.66 mmol). Purification by column chromatography (EtOAc/*n*-hexane 8:2) yielded the title ester **5d** as a white powder (203 mg, 64%); $R_f = 0.68$ (EtOAc/*n*-hexane 8:2). ^{1}H NMR (300 MHz, $CDCl_3$): δ 2.89 (t, 2H, $J = 6.2$ Hz), 3.67 (s, 3H), 4.26 (t, 2H, $J = 6.2$ Hz), 6.48 (d, 1H, $J = 7.3$ Hz), 7.21 (d, 1H, $J = 7.3$ Hz), 7.46–7.51 (m, 2H), 7.63 (td, 1H, $J = 8.1$, 1.1 Hz), 8.41 (d, 1H, $J = 8.1$ Hz).

*4.1.1.5. (6,7-Dimethoxy-1-oxo-1H-isoquinolin-2-yl)acetic acid ethyl ester (**5e**).* Compound **5e** was obtained following the same procedure reported for compound **5c**, using commercially available 6,7-Dimethoxy-isoquinolin-1(2*H*)-one **4d** (200 mg, 0.97 mmol), ethyl 2-bromoacetate (151 μL, 1.36 mmol) and NaH (28 mg, 1.16 mmol). Purification by column chromatography (EtOAc/*n*-hexane 8:2) yielded the title ester **5e** as a white solid (172 mg, 61%); $R_f = 0.50$ (EtOAc/*n*-hexane 8:2). ^{1}H NMR (300 MHz, $CDCl_3$): δ 1.29 (t, 3H, $J = 7.0$ Hz), 3.99 (s, 6H), 4.25 (q, 2H, $J = 7.0$ Hz), 4.70 (s, 2H), 6.45 (d, 1H, $J = 7.0$ Hz), 6.88 (s, 1H), 6.94 (d, 1H, $J = 7.0$ Hz), 7.79 (s, 1H).

*4.1.1.6. 3-(6,7-Dimethoxy-1-oxo-1H-isoquinolin-2-yl)propionic acid methyl ester (**5f**).* Compound **5f** was obtained following the same procedure reported for compound **5a**, using **4d** (200 mg, 0.97 mmol), methyl 3-bromopropionate (212 μL, 1.94 mmol) and KH (46 mg, 1.16 mmol). Purification by column chromatography (EtOAc) yielded the title ester **5f** as a pale yellow solid (151 mg, 54%); $R_f = 0.55$ (EtOAc). ^{1}H NMR (300 MHz, $CDCl_3$): δ 3.58 (t, 2H, $J = 6.4$ Hz), 3.73 (s, 3H), 3.98 (s, 3H), 3.99 (s, 3H), 4.25 (t, 2H, $J = 6.4$ Hz), 6.39 (d, 1H, $J = 7.0$ Hz), 6.85 (s, 1H), 7.13 (d, 1H, $J = 7.0$ Hz), 7.78 (s, 1H).

*4.1.1.7. (7-Bromo-1-oxo-1H-isoquinolin-2-yl)acetic acid ethyl ester (**5g**).* Compound **5g** was obtained following the same procedure reported for compound **5c**, using commercially available 7-Bromo-isoquinolin-1(2*H*)-one **4e** (200 mg, 0.89 mmol), ethyl 2-bromoacetate (139 μL, 1.25 mmol) and NaH (26 mg, 1.07 mmol). Purification by column chromatography (EtOAc/*n*-hexane 6:4) yielded the title ester **5g** as a pale yellow solid (229 mg, 83%); $R_f = 0.68$ (EtOAc/*n*-hexane 6:4). ^{1}H NMR (300 MHz, $CDCl_3$): δ 1.29 (t, 3H, $J = 7.0$ Hz), 4.25 (q, 2H, $J = 7.0$ Hz), 4.69 (s, 2H), 6.49 (d, 1H, $J = 7.6$ Hz), 7.02 (d, 1H, $J = 7.6$ Hz), 7.39 (d, 1H, $J = 8.8$ Hz), 7.71 (dd, 1H, $J = 8.8$, 1.8 Hz), 8.54 (d, 1H, $J = 1.8$ Hz).

*4.1.1.8. 3-(7-Bromo-1-oxo-1H-isoquinolin-2-yl)propionic acid methyl ester (**5h**).* Compound **5h** was obtained following the same procedure reported for compound **5a**, using **4e** (250 mg, 1.12 mmol), methyl 3-bromopropionate (244 μL, 2.24 mmol) and KH (54 mg, 1.34 mmol). Purification by column chromatography ($CHCl_3$/MeOH 98:2) yielded the title ester **5h** as a pale yellow solid (105 mg, 30%); $R_f = 0.67$ ($CHCl_3$/MeOH 98:2). ^{1}H NMR (300 MHz, $CDCl_3$): δ 3.58 (t, 2H, $J = 7.0$ Hz), 3.67 (s, 3H), 4.25 (t, 2H, $J = 7.0$ Hz), 6.44 (d, 1H, $J = 7.0$ Hz), 7.25 (d, 1H, $J = 7.0$ Hz), 7.39 (d, 1H, $J = 8.3$ Hz), 7.72 (d, 1H, $J = 8.3$ Hz), 8.55 (s, 1H).

*4.1.1.9. 3-(5-Oxo-5H-1,6-naphthyridin-6-yl)propionic acid (**6a**).* A cooled solution (0 °C) of **5a** (183 mg, 0.79 mmol) in MeOH (10 mL), was treated with 1 N LiOH (1.6 mL), and the mixture was stirred at room temperature for 6 h. After concentration in vacuo, 6 N HCl was added to the residual aqueous solution (pH ~ 6.8). Upon evaporation of water at reduced pressure, the residue was purified by column chromatography (3% HCOOH in $CHCl_3$/MeOH 9:1) to yield the title compound **6a** as a white powder (168 mg, 97%); $R_f = 0.73$ (3% HCOOH in $CHCl_3$/MeOH 9:1). ^{1}H NMR (300 MHz, DMSO-d_6): δ 2.69 (t, 2H, $J = 6.6$ Hz), 4.14 (t, 2H, $J = 6.6$ Hz), 6.67 (d, 1H, $J = 7.0$ Hz), 7.49 (dd, 1H, $J = 7.6$, 4.4 Hz), 7.73 (d, 1H, $J = 7.0$ Hz), 8.51 (d, 1H, $J = 7.6$ Hz), 8.90 (s, 1H).

*4.1.1.10. 3-(8-Bromo-5-Oxo-5H-1,6-naphthyridin-6-yl)propionic acid (**6b**).* The hydrolysis of the ester intermediate **5b** (150 mg, 0.48 mmol) was carried out applying the same procedure of **6a**, using LiOH (1 mL) to provide a crude which was purified by column chromatography (3% HCOOH in $CHCl_3$/MeOH 9:1) to yield the carboxylic acid **6b** as a white powder (101 mg, 70%); $R_f = 0.41$ (3% HCOOH in $CHCl_3$/MeOH 9:1). ^{1}H NMR (300 MHz, DMSO-d_6): δ 2.69 (t, 2H, $J = 6.97$ Hz), 4.16 (t, 2H, $J = 6.97$ Hz), 7.61 (dd, 1H, $J = 8.07$, 4.40 Hz), 8.22 (s, 1H), 8.56 (dd, 1H, $J = 8.07$, 1.47 Hz), 9.02 (dd, 1H, $J = 4.40$, 1.47 Hz).

*4.1.1.11. (1-Oxo-1H-isoquinolin-2-yl)acetic acid (**6c**).* The hydrolysis of the ester intermediate **5c** (220 mg, 0.95 mmol) was carried out applying the same procedure of **6a**, using LiOH (1.9 mL) and EtOH (10 mL) as solvent. After concentration in vacuo, the residual aqueous solution was treated with 6 N HCl (pH ~ 2) and extracted with EtOAc to provide the pure carboxylic acid **6c** as a white powder (171 mg, 89%); $R_f = 0.14$ ($CHCl_3$/MeOH 9:1). ^{1}H NMR (300 MHz, DMSO-d_6): δ 4.65 (s, 2H), 6.60 (d, 1H, $J = 7.0$ Hz), 7.41 (d, 1H, $J = 7.0$ Hz), 7.46–7.51 (m, 1H), 7.62–7.72 (m, 2H), 8.16 (d, 1H, $J = 8.2$ Hz).

*4.1.1.12. 3-(1-Oxo-1H-isoquinolin-2-yl)propionic acid (**6d**).* The hydrolysis of the ester intermediate **5d** (203 mg, 0.88 mmol) was carried out applying the same procedure of **6c**, using LiOH (1.8 mL) and MeOH (10 mL) as solvent, to provide the pure carboxylic acid **6d** as a white powder (172 mg, 90%); $R_f = 0.29$ ($CHCl_3$/MeOH 9:1). ^{1}H NMR (300 MHz, DMSO-d_6): δ 2.69 (t, 2H, $J = 7.0$ Hz), 4.13 (t, 2H, $J = 7.0$ Hz), 6.59 (d, 1H, $J = 7.3$ Hz), 7.45 (d, 1H, $J = 7.3$ Hz), 7.49 (t, 1H, $J = 8.1$ Hz), 7.63 (d, 1H, $J = 8.1$ Hz), 7.69 (t, 1H, $J = 8.1$ Hz), 8.20 (d, 1H, $J = 8.1$ Hz).

*4.1.1.13. (6,7-Dimethoxy-1-oxo-1H-isoquinolin-2-yl)acetic acid (**6e**).* The hydrolysis of the ester intermediate **5e** (172 mg, 0.59 mmol) was carried out applying the same procedure of **6c**, using LiOH (1.2 mL), to provide the pure carboxylic acid **6e** as a yellow powder (124 mg, 80%); $R_f = 0.23$ ($CHCl_3$/MeOH 9:1). ^{1}H NMR (300 MHz, DMSO-d_6): δ 3.83 (s, 3H), 3.87 (s, 3H), 4.64 (s, 2H), 6.51 (d, 1H, $J = 7.0$ Hz), 7.14 (s, 1H), 7.30 (d, 1H, $J = 7.0$ Hz), 7.53 (s, 1H).

*4.1.1.14. 3-(6,7-Dimethoxy-1-oxo-1H-isoquinolin-2-yl)propionic acid (**6f**).* The hydrolysis of the ester intermediate **5f** (151 mg, 0.52 mmol) was carried out applying the same procedure of **6c**, using LiOH (1 mL) and MeOH (10 mL) as solvent, to provide the pure carboxylic acid **6f** as a pale yellow powder (116 mg, 81%); $R_f = 0.24$ ($CHCl_3$/MeOH 9:1). ^{1}H NMR (300 MHz, DMSO-d_6): δ 2.65 (t, 2H, $J = 7.0$ Hz), 3.83 (s, 3H), 3.85 (s, 3H), 4.09 (t, 2H, $J = 7.0$ Hz), 6.49 (d, 1H, $J = 7.5$ Hz), 7.11 (s, 1H), 7.31 (d, 1H, $J = 7.5$ Hz), 7.54 (s, 1H).

*4.1.1.15. (7-Bromo-1-oxo-1H-isoquinolin-2-yl)acetic acid (**6g**).* The hydrolysis of the ester intermediate **5g** (229 mg, 0.74 mmol) was carried out applying the same procedure of **6c**, using LiOH (1.5 mL), to provide the pure carboxylic acid **6g** as a white powder (203 mg, 97%); $R_f = 0.13$ ($CHCl_3$/MeOH 9:1). ^{1}H NMR (300 MHz, DMSO-d_6): δ 4.67 (s, 2H), 8.65 (d, 1H, $J = 7.0$ Hz), 7.49 (d, 1H, $J = 7.0$ Hz), 7.65 (d, 1H, $J = 8.8$ Hz), 7.87 (d, 1H, $J = 8.8$ Hz), 8.26 (s, 1H).

*4.1.1.16. 3-(7-Bromo-1-oxo-1H-isoquinolin-2-yl)propionic acid (**6h**).* The hydrolysis of the ester intermediate **5h** (105 mg, 0.34 mmol) was carried out applying the same procedure of **6c**, using LiOH (0.7 mL) and MeOH (10 mL) as solvent, to provide the pure carboxylic acid **6h** as a white powder (89 mg, 88%); $R_f = 0.25$ ($CHCl_3$/MeOH 9:1). ^{1}H NMR (300 MHz, DMSO-d_6): δ 2.70 (t, 2H, $J = 7.0$ Hz), 4.14 (t, 2H, $J = 7.0$ Hz), 6.64 (d, 1H, $J = 7.0$ Hz), 7.53 (d, 1H, $J = 7.0$ Hz), 7.64 (d, 1H, $J = 8.3$ Hz), 7.87 (d, 1H, $J = 8.3$ Hz), 8.29 (s, 1H).

*4.1.1.17. R-1-[3-(5-Oxo-5H-1,6-naphthyridin-6-yl)propanamido]-3-methylbutylboronic acid pinanediol ester (**8a**).* A suspension of carboxylic acid **6a** (168 mg, 0.77 mmol) in dry CH_2Cl_2 was cooled to −5 °C and HOBt was added (250 mg, 1.85 mmol). After 20 min, the reaction mixture was further cooled to −15 °C and treated with EDC·HCl (355 mg, 1.85 mmol). Finally, a cold solution of pinandiol L-leucine boronate trifluoroacetate salt **7** in dry CH_2Cl_2 (292 mg, 0.77 mmol) and DIPEA (160 μL, 0.92 mmol) were added in sequence and the reaction mixture was stirred at −15 °C for 1 h and then at room temperature for 2 h. Then, the organic layer was washed with 0.1 M $KHSO_4$, 5% $NaHCO_3$, and brine, dried over Na_2SO_4, filtered, and finally evaporated to give a crude that was triturated in Et_2O and filtered, to afford the amide by-product (**9a**) as a solid. The ether solution was evaporated to give crude **8a** which was used in the next reaction without further purification (293 mg, 82%); $R_f = 0.61$ ($CHCl_3$/MeOH 9:1).

*4.1.1.18. R-1-[3-(8-Bromo-5-oxo-5H-1,6-naphthyridin-6-yl)propanamido]-3-methylbutylboronic acid pinandiol ester (**8b**).* Carboxylic acid **6b** (101 mg, 0.34 mmol) was reacted with HOBt (111 mg, 0.82 mmol), EDC·HCl (157 mg, 0.82 mmol), pinandiol L-leucine boronate **7** (129 mg, 0.34 mmol) and DIPEA (71 μL, 0.41 mmol) following the same procedure reported for **8a**, to give the amide by-product (**9b**) and the crude **8b** (169 mg, 90%); $R_f = 0.63$ ($CHCl_3$/MeOH 9:1).

*4.1.1.19. R-1-[(1-Oxo-1H-isoquinolin-2-yl)acetamido]-3-methylbutylboronic acid pinandiol ester (**8c**).* Carboxylic acid **6c** (171 mg, 0.84 mmol) was reacted with HOBt (273 mg, 2.02 mmol), EDC·HCl (387 mg, 2.02 mmol), pinandiol L-leucine boronate **7** (318 mg, 0.84 mmol) and DIPEA (175 μL, 1.01 mmol) following the same procedure reported for **8a**, to give the amide by-product (**9c**) and the crude **8c** (275 mg, 73%); $R_f = 0.79$ ($CHCl_3$/MeOH 9:1).

*4.1.1.20. R-1-[3-(1-Oxo-1H-isoquinolin-2-yl)propanamido]-3-methylbutylboronic acid pinandiol ester (**8d**).* Carboxylic acid **6d** (172 mg, 0.79 mmol) was reacted with HOBt (257 mg, 1.90 mmol), EDC·HCl (364 mg, 1.90 mmol), pinandiol L-leucine boronate **7** (300 mg, 0.79 mmol) and DIPEA (166 μL, 0.95 mmol) following the same procedure reported for **8a**, to give the amide by-product (**9d**) and the crude **8d** (330 mg, 90%); $R_f = 0.77$ ($CHCl_3$/MeOH 9:1).

*4.1.1.21. R-1-[(6,7-Dimethoxy-1-oxo-1H-isoquinolin-2-yl)acetamido]-3-methylbutylboronic acid pinandiol ester (**8e**).* Carboxylic acid **6e** (124 mg, 0.47 mmol) was reacted with HOBt (153 mg, 1.13 mmol), EDC·HCl (217 mg, 1.13 mmol), pinandiol L-leucine boronate **7** (178 mg, 0.47 mmol) and DIPEA (97 μL, 0.56 mmol) following the same procedure reported for **8a**, to give the amide by-product (**9e**) and the crude **8e** (179 mg, 74%); $R_f = 0.85$ ($CHCl_3$/MeOH 9:1).

*4.1.1.22. R-1-[3-(6,7-Dimethoxy-1-oxo-1H-isoquinolin-2-yl)propanamido]-3-methylbutylboronic acid pinandiol ester (**8f**).* Carboxylic acid **6f** (116 mg, 0.42 mmol) was reacted with HOBt (136 mg, 1.01 mmol), EDC·HCl (194 mg, 1.01 mmol), pinandiol L-leucine boronate **7** (159 mg, 0.42 mmol) and DIPEA (88 μL, 0.50 mmol) following the same procedure reported for **8a**, to give the amide by-product (**9f**) and the crude **8f** (121 mg, 56%); $R_f = 0.87$ ($CHCl_3$/MeOH 9:1).

*4.1.1.23. R-1-[(7-Bromo-1-oxo-1H-isoquinolin-2-yl)acetamido]-3-methylbutylboronic acid pinandiol ester (**8g**).* Carboxylic acid **6g** (203 mg, 0.72 mmol) was reacted with HOBt (234 mg, 1.73 mmol), EDC·HCl (332 mg, 1.73 mmol), pinandiol L-leucine boronate **7** (273 mg, 0.72 mmol) and DIPEA (150 μL, 0.86 mmol) following the same procedure reported for **8a**, to give the amide by-product (**9g**) and the crude **8g** (275 mg, 72%); $R_f = 0.81$ ($CHCl_3$/MeOH 9:1).

*4.1.1.24. R-1-[3-(7-Bromo-1-oxo-1H-isoquinolin-2-yl)propanamido]-3-methylbutylboronic acid pinandiol ester (**8h**).* Carboxylic acid **6h** (89 mg, 0.30 mmol) was reacted with HOBt (97 mg, 0.72 mmol), EDC·HCl (138 mg, 0.72 mmol), pinandiol L-leucine boronate **7** (114 mg, 0.30 mmol) and DIPEA (62 μL, 0.36 mmol) following the same procedure reported for **8a**, to give the amide by-product (**9h**) and the crude **8h** (125 mg, 77%); $R_f = 0.83$ ($CHCl_3$/MeOH 9:1).

*4.1.1.25. R-1-[3-(5-Oxo-5H-1,6-naphthyridin-6-yl)propanamido]-3-methylbutylboronic acid (**2a**).* To a solution of crude compound **8a** (293 mg, 0.63 mmol) in MeOH/*n*-hexane (1:1, 11.4 mL), isobutylboronic acid (321 mg, 3.15 mmol) was added and the reaction mixture was treated with 1 N HCl (1.6 mL), and stirred at room temperature for 18 h. The methanolic phase was washed with *n*-hexane (3× 10 mL) and the combined *n*-hexane layers with MeOH (3× 10 mL). After concentration in vacuo of the collected methanolic phase, the obtained residue was dissolved in CH_2Cl_2 and washed with 5% $NaHCO_3$. The aqueous phase was extracted with $CHCl_3$ and the organic phase was evaporated in vacuo to give a solid that was purified by trituration with Et_2O to give the title product **2a** as a white powder (63 mg, 30%); $R_f = 0.14$ ($CHCl_3$/MeOH 9:1); $[\alpha_D^{26}] = -16.7$ (*c* 0.4, MeOH); ^{1}H NMR (300 MHz, CD_3OD): δ 0.75 (d, 6H, $J = 6.4$ Hz), 1.05–1.15 (m, 2H), 1.25–1.45 (m, 1H), 2.75–2.95 (m, 2H), 3.10–3.25 (m, 1H), 4.15–4.35 (m, 2H), 4.50 (bs, 1H), 6.70 (d, 1H, $J = 7.0$ Hz), 7.43–7.50 (m, 1H), 7.55 (d. 1H, $J = 7.0$ Hz), 8.60 (d, 1H, $J = 7.6$ Hz), 8.82 (bs, 1H). ^{13}C NMR (75 MHz, CD_3OD): δ 20.8, 22.7, 25.7, 29.4, 39.7, 45.7, 48.7, 107.0, 121.8, 122.2, 136.4, 137.1, 153.5, 154.5, 162.3, 176.0. MS (ESI) *m/z* 330.0 $[M - H]^-$ (100%). Anal. Calcd. for $C_{16}H_{22}BN_3O_4$: C 58.03, H 6.70, N 12.69. Found: C 58.12, H 6.72, N 12.65.

*4.1.1.26. R-1-[3-(8-Bromo-5-oxo-5H-1,6-naphthyridin-6-yl)propanamido]-3-methylbutylboronic acid (**2b**).* Synthesis of compound **2b** was performed following the same procedure described for compound **2a** using **8b** (169 mg, 0.31 mmol), isobutylboronic acid (158 mg, 1.55 mmol), 1 N HCl (0.8 mL) and a mixture of MeOH and *n*-hexane as solvent (1:1, 5.6 mL). Purification by flash chromatography ($CHCl_3$/MeOH 9:1) yielded the title compound **2b** as a pale yellow solid (37 mg, 29%); $R_f = 0.42$ ($CHCl_3$/MeOH 9:1); $[\alpha_D^{26}] = -12.8$ (*c* 0.3, MeOH); ^{1}H NMR (300 MHz, CD_3OD): δ 0.82 (d, 6H, $J = 6.1$ Hz), 1.12–1.23 (m, 2H), 1.44–1.57 (m, 1H), 2,73 (t, 2H, $J = 6.4$ Hz), 3.10–3.27 (m, 1H), 4.20 (t, 2H, $J = 6.4$ Hz), 7.44 (m, 1H), 8.06 (s, 1H), 8.69 (d, 1H, $J = 7.6$ Hz), 8.98 (d, 1H, $J = 4.4$ Hz). ^{13}C NMR (75 MHz, CD_3OD): δ 20.8, 23.1, 25.9, 29.5, 39.5, 45.6, 48.8, 103.9, 121.0, 122.1, 136.0, 138.4, 154.1, 155.4, 162.7, 173.4. MS (ESI) *m/z* 409.3 $[M - H]^-$ (100%). Anal. Calcd. for $C_{16}H_{21}BBrN_3O_4$: C 46.86, H 5.16, N 10.25. Found: C 46.81, H 5.17, N 10.28.

*4.1.1.27. R-1-[(1-Oxo-1H-isoquinolin-2-yl)acetamido]-3-methylbutylboronic acid (**3a**).* Synthesis of compound **3a** was performed following the same procedure described for compound **2a** using **8c** (275 mg, 0.61 mmol), isobutylboronic acid (311 mg,

3.05 mmol), 1 N HCl (1.6 mL) and a mixture of MeOH and *n*-hexane as solvent (1:1, 11 mL). Purification by flash chromatography ($CHCl_3$/MeOH 9:1 till all impurities came off, then 100% MeOH to elute the product) yielded the title compound **3a** as a white solid (53 mg, 28%); $R_f = 0.29$ (MeOH); $[\alpha_D^{26}] = -90.0$ (*c* 0.1, MeOH); ^{1}H NMR (300 MHz, CD_3OD): δ 0.91 (d, 6H, $J = 6.4$ Hz), 1.34–1.41 (m, 2H), 1.62–1.69 (m, 1H), 2.75–2.85 (m, 1H), 4.88 (s, 2H), 6.70 (d, 1H, $J = 7.2$ Hz), 7.35 (d, 1H, $J = 7.2$ Hz), 7.52 (t, 1H, $J = 7.2$ Hz), 7.62–7.74 (m, 2H), 8.27 (d, 1H, $J = 7.9$ Hz). ^{13}C NMR (75 MHz, CD_3OD): δ 21.0, 22.3, 25.6, 39.5, 46.8, 48.5, 106.8, 125.2, 126.2, 126.8, 132.3, 132.6, 135.3, 137.7, 161.7, 174.0. MS (ESI) *m/z* 315.0 $[M - H]^-$ (100%). Anal. Calcd. for $C_{16}H_{21}BN_2O_4$: C 60.78, H 6.69, N 8.86. Found: 60.59, H 6.71, N 8.88.

*4.1.1.28. R-1-[3-(1-Oxo-1H-isoquinolin-2-yl)propanamido]-3-methylbutylboronic acid (**3b**).* Synthesis of compound **3b** was performed following the same procedure described for compound **2a** using **8d** (330 mg, 0.71 mmol), isobutylboronic acid (362 mg, 3.55 mmol), 1 N HCl (1.8 mL) and a mixture of MeOH and *n*-hexane as solvent (1:1, 12.8 mL) to yield the title compound **3b** as a white solid (82 mg, 35%); $R_f = 0.25$ ($CHCl_3$/MeOH 9:1); $[\alpha_D^{26}] = -12.0$ (*c* 0.2, MeOH); ^{1}H NMR (300 MHz, CD_3OD): δ 0.79 (d, 3H, $J = 6.4$ Hz), 0.81 (d, 3H, $J = 6.4$ Hz), 1.18–1.27 (m, 2H), 1.39–1.51 (m, 1H), 2.56–2.61 (m, 1H), 2.93–2.99 (m, 2H), 4.25–4.45 (m, 2H), 6.68 (d, 1H, $J = 7.2$ Hz), 7.73 (d, 1H, $J = 7.2$ Hz), 7.52 (t, 1H, $J = 7.0$ Hz), 7.61–7.73 (m, 2H), 8.30 (d, 1H, $J = 7.9$ Hz). ^{13}C NMR (125 MHz, CD_3OD): δ 20.5, 22.4, 25.4, 29.4, 39.4, 45.4, 48.2, 106.7, 125.3, 126.0, 126.7, 132.2, 132.4, 135.5, 137.5, 162.5, 175.9. MS (ESI) *m/z* 329.0 $[M - H]^-$ (100%). Anal. Calcd. for $C_{17}H_{23}BN_2O_4$: C 61.84, H 7.02, N 8.48. Found: C 61.63, H 7.03, N 8.50.

*4.1.1.29. R-1-[(6,7-Dimethoxy-1-oxo-1H-isoquinolin-2-yl)acetamido]-3-methylbutylboronic acid (**3c**).* Synthesis of compound **3c** was performed following the same procedure described for compound **2a** using **8e** (179 mg, 0.35 mmol), isobutylboronic acid (178 mg, 1.75 mmol), 1 N HCl (0.9 mL) and a mixture of MeOH and *n*-hexane as solvent (1:1, 6.2 mL). Purification by flash chromatography ($CHCl_3$/MeOH 9:1) yielded the title compound **3c** as a white solid (38 mg, 29%); $R_f = 0.28$ ($CHCl_3$/MeOH 9:1); $[\alpha_D^{26}] = -6.0$ (*c* 0.1, DMSO); ^{1}H NMR (300 MHz, DMSO-d_6): δ 0.85 (d, 3H, $J = 6.4$ Hz), 0.88 (d, 3H, $J = 6.4$ Hz), 1.33–1.46 (m, 2H), 1.60–1.68 (m, 1H), 2.50–2.59 (m, 1H), 3.85 (s, 3H), 3.89 (s, 3H), 4.55 (s, 2H), 5.22 (bs, 1H), 6.50 (d, 1H, $J = 7.6$ Hz), 7.15 (s, 1H), 7.24 (d, 1H, $J = 7.6$ Hz), 7.54 (s, 1H). ^{13}C NMR (75 MHz, DMSO-d_6): δ 23.0, 23.4, 24.7, 38.6, 46.0, 51.4, 56.2, 56.4, 104.7, 107.3, 107.6, 119.7, 132.7, 133.4, 149.2, 153.7, 161.1, 167.3. MS (ESI) *m/z* 377.1 $[M + H]^+$ (100%). Anal. Calcd. for $C_{18}H_{25}BN_2O_6$: C 57.47, H 6.70, N 7.45. Found: C 57.58, H 6.68, N 7.47.

*4.1.1.30. R-1-[3-(6,7-Dimethoxy-1-oxo-1H-isoquinolin-2-yl)propanamido]-3-methylbutylboronic acid (**3d**).* Synthesis of compound **3d** was performed following the same procedure described for compound **2a** using **8f** (121 mg, 0.23 mmol), isobutylboronic acid (117 mg, 1.15 mmol), 1 N HCl (0.6 mL) and a mixture of MeOH and *n*-hexane as solvent (1:1, 4.2 mL) to yield the title compound **3d** as a white solid (31 mg, 33%); $R_f = 0.22$ ($CHCl_3$/MeOH 9:1); $[\alpha_D^{26}] = -10.0$ (*c* 0.2, MeOH); ^{1}H NMR (300 MHz, $CDCl_3$): δ 0.75 (d, 3H, $J = 6.6$ Hz), 0.77 (d, 3H, $J = 6.6$ Hz), 1.27–1.39 (m, 2H), 1.45–1.54 (m, 1H), 2.68–2.87 (m, 3H), 3.88 (s, 3H), 3.94 (s, 3H), 4.25–4.32 (m, 2H), 6.40 (d, 1H, $J = 7.0$ Hz), 6.80 (s, 1H), 7.06 (d, 1H, $J = 7.0$ Hz), 7.46 (s, 1H), 8.27 (bs, 1H). ^{13}C NMR (75 MHz, $CDCl_3$): δ 22.6, 23.1, 25.9, 29.6, 33.3, 40.0, 45.0, 55.9, 56.2, 105.0, 106.7, 107.2, 119.5, 131.8, 132.7, 149.2, 153.5, 161.8, 172.9. MS (ESI) *m/z* 391.3 $[M + H]^+$ (100%). Anal. Calcd. for $C_{19}H_{27}BN_2O_6$: C 58.48, H 6.97, N 7.18. Found: C 58.37, H 6.95, N 7.20.

*4.1.1.31. R-1-[(7-Bromo-1-oxo-1H-isoquinolin-2-yl)acetamido]-3-methylbutylboronic acid (**3e**).* Synthesis of compound **3e** was performed following the same procedure described for compound **2a** using **8g** (275 mg, 0.52 mmol), isobutylboronic acid (265 mg, 2.6 mmol), 1 N HCl (1.3 mL) and a mixture of MeOH and *n*-hexane as solvent (1:1, 9.4 mL), to yield the title compound **3e** as a white solid (75 mg, 36%); $R_f = 0.31$ ($CHCl_3$/MeOH 9:1); $[\alpha_D^{26}] = -31.5$ (*c* 0.2, *i*-PrOH); ^{1}H NMR (300 MHz, DMSO-d_6): δ 0.84 (d, 3H, $J = 7.0$ Hz), 0.86 (d, 3H, $J = 7.0$ Hz), 1.13–1.23 (m, 2H), 1.46–1.57 (m, 1H), 3.08–3.15 (m, 1H), 4.76 (s, 2H), 6.66 (d, 1H, $J = 7.0$ Hz), 7.45 (d, 1H, $J = 7.0$ Hz), 7.65 (d, 1H, $J = 8.8$ Hz), 7.88 (d, 1H, $J = 8.8$ Hz), 8.28 (s, 1H). ^{13}C NMR (75 MHz, CD_3OD): δ 21.2, 22.5, 25.8, 32.9, 39.7, 46.9, 106.2, 120.5, 126.9, 128.4, 129.5, 133.2, 135.8, 136.7, 161.7, 172.4. MS (ESI) *m/z* 394.1 $[M - H]^-$ (100%). Anal. Calcd. for $C_{16}H_{20}BBrN_2O_4$: C 48.64, H 5.10, N 7.09. Found: C 48.59, H 5.11, N 7.07.

*4.1.1.32. R-1-[3-(7-Bromo-1-oxo-1H-isoquinolin-2-yl)propanamido]-3-methylbutylboronic acid (**3f**).* Synthesis of compound **3f** was performed following the same procedure described for compound **2a** using **8h** (125 mg, 0.23 mmol), isobutylboronic acid (117 mg, 1.15 mmol), 1 N HCl (0.6 mL) and a mixture of MeOH and *n*-hexane as solvent (1:1, 4.2 mL), to yield the title compound **3f** as a white solid (29 mg, 30%); $R_f = 0.10$ ($CHCl_3$/MeOH 9:1); $[\alpha_D^{26}] = -3.0$ (*c* 0.2, MeOH); ^{1}H NMR (300 MHz, $CDCl_3$). δ 0.82 (s, 6H), 1.41–1.53 (m, 2H), 1.74–1.93 (m, 1H), 2.69–2.98 (m + s, 3H), 4.31 (t, 2H, $J = 7.0$ Hz), 6.52 (d, 1H, $J = 7.0$ Hz), 7.22 (d, 1H, $J = 7.0$ Hz), 7.41 (d, 1H, $J = 8.2$ Hz), 7.65 (d, 1H, $J = 8.2$ Hz), 7.98 (bs, 1H), 8.26 (s, 1H). ^{13}C NMR (75 MHz, $CDCl_3$): δ 22.7, 23.0, 25.9, 29.7, 33.0, 40.1, 45.4, 106.4, 120.8, 126.9, 127.8, 129.9, 132.5, 135.7, 135.8, 161.4, 172.8. MS (ESI) *m/z* 410.1 $[M + H]^+$ (100%). Anal. Calcd. for $C_{17}H_{22}BBrN_2O_4$: C 49.91, H 5.42, N 6.85. Found: C 49.85, H 5.44, N 6.87.

*4.1.2. Characterization of amide by-products **9***

*4.1.2.1. N-Isopentyl-3-(5-oxo-5H-1,6-naphthyridin-6-yl)propanamide (**9a**).* Yield 16%. $R_f = 0.50$ ($CHCl_3$/MeOH 9:1). ^{1}H NMR (300 MHz, $CDCl_3$): δ 0.80 (d, 6H, $J = 6.4$ Hz), 1.23–1.30 (m, 2H), 1.38–1.49 (m, 1H), 2.69–2.71 (m, 2H), 3.17–3.24 (m, 2H), 4.29–4.33 (m, 2H), 5.76 (bs, 1H), 6.74 (d, 1H, $J = 7.6$ Hz), 7.37 (d, 1H, $J = 7.6$ Hz), 7.48 (d, 1H, $J = 7.6$ Hz), 8.60 (d, 1H, $J = 7.6$ Hz), 8.88 (s, 1H). Anal. Calcd. for $C_{16}H_{21}N_3O_2$: C 66.88, H 7.37, N 14.62; found: C 66.95, H 7.39, N 14.68.

*4.1.2.2. N-Isopentyl-3-(8-bromo-5-oxo-5H-1,6-naphthyridin-6-yl) propanamide (**9b**).* Yield 9%. $R_f = 0.57$ ($CHCl_3$/MeOH 9:1). ^{1}H NMR (300 MHz, $CDCl_3$): δ 0.83 (d, 6H, $J = 6.4$ Hz), 1.27–1.35 (m, 2H), 1.41–1.48 (m, 1H), 2.69–2.79 (m, 2H), 3.13–3.25 (m, 2H), 4.27–4.31 (m, 2H), 6.14 (bs, 1H), 7.48 (dd, 1H, $J = 7.6$, 4.1 Hz), 7.85 (s, 1H), 8.66 (d, 1H, $J = 7.6$ Hz), 9.04 (d, 1H, $J = 4.1$ Hz). Anal. Calcd. for $C_{16}H_{20}BrN_3O_2$: C 52.47, H 5.50, N 11.47; found: C 52.40, H 5.51, N 11.45.

*4.1.2.3. N-Isopentyl-2-(1-oxo-1H-isoquinolin-2-yl)acetamide (**9c**).* Yield 15%. $R_f = 0.64$ ($CHCl_3$/MeOH 9:1). ^{1}H NMR (300 MHz, $CDCl_3$): δ 0.85 (d, 6H, $J = 5.2$ Hz), 1.35–1.39 (m, 2H), 1.51–1.59 (m, 1H), 3.18–3.29 (m, 2H), 4.62 (s, 2H), 6.53 (d, 1H, $J = 7.3$ Hz), 7.01 (d, 1H, $J = 7.3$ Hz), 7.48–7.53 (m, 2H), 7.65 (t, 1H, $J = 8.1$ Hz), 8.42 (d, 1H, $J = 8.1$ Hz). Anal. Calcd. for $C_{16}H_{20}N_2O_2$: C 70.56, H 7.40, N 10.29; found: C 70.79, H 7.38, N 10.27.

*4.1.2.4. N-Isopentyl-3-(1-oxo-1H-isoquinolin-2-yl)propanamide (**9d**).* Yield 8%. $R_f = 0.75$ ($CHCl_3$/MeOH 9:1). ^{1}H NMR (300 MHz, $CDCl_3$): δ 0.80 (d, 6H, $J = 6.4$ Hz), 1.23–1.30 (m, 2H), 1.43–1.52 (m, 1H), 2.73 (t, 2H, $J = 5.9$ Hz), 3.17–3.24 (m, 2H), 4,29 (t, 2H, $J = 5.9$ Hz), 6.15 (bs, 1H), 6.48 (d, 1H, $J = 7.6$ Hz), 7.22 (d, 1H, $J = 7.6$ Hz), 7.42–7.52 (m, 2H), 7.62 (t, 1H, $J = 8.2$ Hz), 8.33 (d, 1H,

J = 8.2 Hz). Anal. Calcd. for $C_{17}H_{22}N_2O_2$: C 71.30, H 7.74, N 9.78; found: C 71.49, H 7.73, N 9.76.

*4.1.2.5. N-Isopentyl-2-(6,7-dimethoxy-1-oxo-1H-isoquinolin-2-yl) acetamide (**9e**).* Yield 6%. R_f = 0.63 ($CHCl_3$/MeOH 9:1). ^{1}H NMR (300 MHz, $CDCl_3$): δ 0.86 (d, 6H, J = 6.6 Hz), 1.33–1.40 (m, 2H), 1.50–1.63 (m, 1H), 3.20–3.27 (m, 2H), 4.00 (s, 3H), 4.01 (s, 3H), 4.60 (s, 2H), 6.50 (d, 1H, J = 7.5 Hz), 6.71 (bs, 1H), 6.90 (s, 1H), 7.11 (d, 1H, J = 7.5 Hz), 7.77 (s, 1H). Anal. Calcd. for $C_{18}H_{24}N_2O_4$: C 65.04, H 7.28, N 8.43; found: C 65.19, H 7.24, N 8.41.

*4.1.2.6. N-Isopentyl-3-(6,7-dimethoxy-1-oxo-1H-isoquinolin-2-yl) propionamide (**9f**).* Yield 42%. R_f = 0.65 ($CHCl_3$/MeOH 9:1). ^{1}H NMR (300 MHz, $CDCl_3$): δ 0.74 (d, 6H, J = 6.4 Hz), 1.18–1.26 (m, 2H), 1.36–1.45 (m, 1H), 2.68 (t, 2H, J = 5.9 Hz), 3.10–3.17 (m, 2H), 3.86 (s, 3H), 3.90 (s, 3H), 4.22 (t, J = 5.9 Hz), 6.31 (d, 1H, J = 7.6 Hz), 6.38 (bs, 1H), 6.75 (s, 1H), 7.06 (s, 1H, J = 7.6 Hz), 7.50 (s, 1H). Anal. Calcd. for $C_{19}H_{26}N_2O_4$: C 65.88, H 7.56, N 8.09; found: C 65.81, H 7.54, N 8.11.

*4.1.2.7. N-Isopentyl-2-(7-bromo-1-oxo-1H-isoquinolin-2-yl)acetamide (**9g**).* Yield 17%. R_f = 0.62 ($CHCl_3$/MeOH 95:5). ^{1}H NMR (300 MHz, DMSO-d_6): δ 0.85 (d, 6H, J = 6.6 Hz), 1.26–1.33 (m, 2H), 1.52–1.62 (m, 1H), 3.04–3.11 (m, 2H), 4.56 (s, 2H), 6.62 (d, 1H, J = 7.1 Hz), 7.42 (d, 1H, J = 7.1 Hz), 7.64 (d, 1H, J = 8.3 Hz), 7.85 (d, 1H, J = 8.3 Hz), 8.12 (bs, 1H), 8.25 (s, 1H). Anal. Calcd. for $C_{16}H_{19}BrN_2O_2$: C 54.71, H 5.46, N 7.98; found: C 54.80, H 7.30, N 7.97.

*4.1.2.8. N-Isopentyl-3-(7-bromo-1-oxo-1H-isoquinolin-2-yl)propionamide (**9h**).* Yield 20%. R_f = 0.55 ($CHCl_3$/MeOH 9:1). ^{1}H NMR (300 MHz, DMSO-d_6): δ 0.76 (d, 6H, J = 7.0 Hz), 1.14–1.21 (m, 2H), 1.34–1.41 (m, 1H), 2.73 (t, 2H, J = 6.4 Hz), 2.97–3.04 (m, 2H), 4.14 (t, 2H, J = 6.4 Hz), 6.61 (d, 1H, J = 7.6 Hz), 7.41 (d, 1H, J = 7.6 Hz), 7.64 (d, 1H, J = 8.2 Hz), 7.82–7.87 (m, 2H), 8.30 (s, 1H). Anal. Calcd. for $C_{17}H_{21}BrN_2O_2$: C 55.90, H 5.79, N 7.67; found: C 55.80, H 5.81, N 7.69.

4.2. Computational chemistry

Molecular modeling and graphics manipulations were performed using Maestro 9.7 (Schrödinger) [23] and UCSF-CHIMERA software packages [24], running on an E4 Computer Engineering E1080 workstation provided of an Intel Core i7-930 Quad-Core processor. GOLD 5.2 [25] was used for all docking calculations. Figures were generated using Pymol 1.0 [26].

4.2.1. Protein and ligands preparation

Atom coordinates of β1 and β5 subunits derived from the X-ray crystal structure of the yeast 20S proteasome determined at 2.8 Å resolution (PDB ID: 2F16) [12] were employed for the automated docking studies.

The protein setup was carried out by Protein Preparation Wizard in Maestro. Hydrogen atoms were added to the protein consistent with the neutral physiologic pH. Arginine and lysine side chains were considered as cationic at the guanidine and ammonium groups, and the aspartic and glutamic residues were considered as anionic at the carboxylate groups. The crystal structure of bortezomib bound to the β5 subunit revealed one well-defined water molecule in proximity to D114O$^{\gamma}$, which coordinates a tight H-bonding network, interacting with β6-D114O$^{\gamma}$, β5-A49N and β5-A50N of the protein and with the C]O oxygen of bortezomib [12]. Moreover, one of the pyrazine nitrogens of bortezomib was found to interact via a direct H-bond with the protonated β6-D114. In fact, it has been observed that the pKa of pyrazine is approximately 1.0 and thus β6-D114 is most likely protonated. This is supported by the fact that in the X-ray structure the O–N distance is 2.9 Å, indicative of a strong H-bond. Accordingly, the intervening water molecule and the proper protonation state of D114 were included in the docking experiments of inhibitors to the β5 active site. The protonation and flip states of the imidazole rings of the histidine residues were adjusted together with the side chain amides of glutamine and asparagine residues in an H-bonding network optimization process. Successively, the protein hydrogens only were minimized using the Impref module of Impact with the OPLS_2005 force field.

The initial structures of inhibitors were created, modified and energy-minimized with Schrödinger's Maestro.

4.2.2. Docking studies

Inhibitors were covalently docked to the binding pocket of both β1 and β5 subunits using GOLD, version 5.2 [25]. A radius of 20 Å from the β1 or β5 catalytic N-terminal threonine was used to direct site location. For each of the genetic algorithm runs, a maximum of 100,000 operations were performed on a population of 100 individuals with a selection pressure of 1.1. As described in the manual of GOLD algorithm, the selection pressure is defined as the ratio between the probability that the most fit member of the population is selected as a parent to the probability that an average member is selected as a parent. Too high a selection pressure will result in the population converging too early. For the GOLD docking algorithm, a selection pressure of 1.1 seems appropriate, although 1.125 may be better for library screening where the aim is faster convergence. Operator weights for crossover, mutation, and migration were set to 95, 95, and 10, respectively, as recommended by the authors of the software. The distance for H-bonding was set to 2.5 Å, and the cutoff value for van der Waals calculation was set to 4 Å. Covalent docking was applied, and the terminal boron atom of inhibitors was bonded to the hydroxyl oxygen of β1-T1 or β5-T1. For docking to the β5 active site, the water molecule near β6-D114 was kept as active water molecule, setting it to "toggle", which means that GOLD decides whether this water is bound or displaced along the docking run [27]. The GoldScore-CS docking protocol [28] was adopted in this study. In this protocol, the poses obtained with the original GoldScore function are rescored and reranked with the GOLD implementation of the ChemScore function [11,28,29]. To perform a thorough and unbiased search of the conformation space, each docking run was allowed to produce 200 poses without the option of early termination, using standard default settings. The top solution obtained after re-ranking of the poses with ChemScore was selected to generate the proteasome/ligand complexes.

4.3. Pharmacology

4.3.1. In vitro 20S proteasome inhibition assays

Human 20S proteasome was obtained from Biomol GmbH, Hamburg, Germany. The three distinct proteolytic activities of the 20S proteasome were measured by monitoring the hydrolysis of the peptidyl 7-amino-4-methyl coumarin substrates (all obtained from Bachem) Suc–Leu–Leu–Val–Tyr–AMC, Boc–Leu–Arg–Arg–AMC, and Cbz–Leu–Leu–Glu–AMC for ChT-L, T-L and PGPH activity of the enzyme, respectively. Fluorescence of the product AMC of the substrates' hydrolyzes was measured using an Infinite 200 PRO microplate reader (Tecan, Männedorf, Switzerland) at 30 °C with a 380 nm excitation filter and a 460 nm emission filter. The preliminary screening for the inhibition of the three proteolytic activities of the 20S proteasome was performed at 20 μM inhibitor concentrations using an equivalent amount of DMSO as a negative control. Compounds showing at least 40% inhibition at 20 μM were subjected to detailed assays. The dissociation constants K_i of the noncovalent complex E·I were obtained from progress curves (10 min) at various concentrations of inhibitor

by fitting the progress curves to a 4 parameter IC_{50} equation, and correction to zero substrate concentration from $K_i = IC_{50}/(1 + [S]K_m^{-1})$. The K_m values were determined in separate experiments: ChT-L activity with Suc–Leu–Leu–Val–Tyr–AMC 13 μM, and PGPH activity with Cbz–Leu–Leu–Glu–AMC 53 μM.

4.3.2. Assaying the chymotryptic activity of the 20S proteasome

Human 20S proteasome was incubated at 30 °C at a final concentration of 0.004 mg mL^{-1} with test compound present at variable concentrations. The reaction buffer consisted of 50 mM Tris pH 7.5, 10 mM NaCl, 25 mM KCl, 1 mM $MgCl_2$, 0.03% SDS, and 5% DMSO. Product release from substrate hydrolysis (75 μM) was monitored continuously over a period of 10 min for amides and 30 min for boronates.

4.3.3. Assaying the tryptic activity of the 20S proteasome

Human 20S proteasome was incubated at 30 °C at a final concentration of 0.0025 mg mL^{-1} at variable concentrations. The reaction buffer consisted of 50 mM Tris buffer pH 7.4, 50 mM NaCl, 0.5 mM EDTA, 0.03% SDS, and 7.5% DMSO. Product release from substrate hydrolysis (85 μM) was monitored continuously over a period of 10 min.

4.3.4. Assaying the post-glutamyl-peptide hydrolyzing activity of the 20S proteasome

Human 20S proteasome was incubated at 30 °C at a final concentration of 0.004 mg mL^{-1} with the test compound present at variable concentrations. The reaction buffer consisted of 50 mM Tris buffer pH 7.5 containing 25 mM KCl, 10 mM NaCl, 1 mM $MgCl_2$, 0.03% SDS, 5% DMSO. Product release from substrate hydrolysis (80 μM) was monitored continuously over a period of 10 min.

4.3.5. Assays for bovine pancreatic α-chymotrypsin inhibition

The enzyme (250 μg mL^{-1}) was incubated at 20 °C with test compound present at variable concentrations. The reaction buffer consisted of 50 mM Tris buffer pH 8.0 containing 100 mM NaCl and 5 mM EDTA and 7.5% DMSO. Product release from substrate hydrolysis (75 μM final concentration, Suc–Leu–Leu–Val–Tyr–AMC from Bachem) was determined over a period of 10 min.

Acknowledgments

This work was financially supported by the Ministero dell'Istruzione, dell'Università e della Ricerca [MIUR-PRIN2010-2011, grants 2010W7YRLZ_003 (A.L.) and 2010W7YRLZ_004 (S.G.)]. We would like to thank the Deutscher Akademischer Austausch Dienst (DAAD) (Vigoni project 2011/12) for partial support of this work. TS thanks the Deutsche Forschungsgemeinschaft (DFG) for financial support. We thank the Division of Cancer Research, National Cancer Institute, Germantown, Maryland, for performing the antitumor tests.

References

[1] M. Groll, L. Ditzel, J. Lowe, M. Bochtler, H.D. Bartunik, R. Huber, Structure of 20S proteasome from yeast at 2.4Å resolution, Nature 386 (1997) 463–471.
[2] M. Groll, W. Heinemeyer, S. Jager, T. Ulrich, M. Bochtler, D.H. Wolf, R. Huber, The catalytic sites of 20S proteasomes and their role in subunit maturation: a mutational and crystallographic study, Proc. Natl. Sci. USA 96 (1999) 10976–10983.
[3] N. Micale, K. Scarbaci, V. Troiano, R. Ettari, S. Grasso, M. Zappalà, Peptide-based proteasome inhibitors in anticancer drug design, Med. Res. Rev. (2014), http://dx.doi.org/10.1002/med.21312.
[4] L. Borissenko, M. Groll, 20S Proteasome and its inhibitors: crystallographic knowledge for drug development, Chem. Rev. 107 (2007) 687–717.
[5] A. Field-Smith, G.J. Morgan, F.E. Davies, Bortezomib (Velcade™) in the treatment of multiple myeloma, Ther. Clin. Risk Manage. 2 (2006) 271–279.
[6] R.C. Kane, R. Dagher, A. Farrell, C.W. Ko, R. Sridhara, R. Justice, R. Pazdur, Bortezomib for the treatment of mantle cell lymphoma, Clin. Cancer Res. 13 (2007) 5291–5294.
[7] N. Micale, A.P. Kozikowski, R. Ettari, S. Grasso, M. Zappalà, J.-J. Jeong, A. Kumar, M. Hanspal, A.H. Chishti, Novel peptidomimetic cysteine protease inhibitors as potential antimalarial agents, J. Med. Chem. 49 (2006) 3064–3067;
(b) R. Ettari, E. Nizi, M.E. Di Francesco, M.A. Dude, G. Pradel, R. Vicik, T. Schirmeister, N. Micale, S. Grasso, M. Zappalà, Development of peptidomimetics with a vinyl sulfone warhead as irreversible falcipain-2 inhibitors, J. Med. Chem. 51 (2008) 988–996;
(c) R. Ettari, E. Nizi, M.E. Di Francesco, N. Micale, S. Grasso, M. Zappalà, R. Vičík, T. Schirmeister, Nonpeptidic vinyl and allyl phosphonates as falcipain-2 inhibitors, ChemMedChem 3 (2008) 1030–1033;
(d) R. Ettari, N. Micale, T. Schirmeister, C. Gelhaus, M. Leippe, E. Nizi, M.E. Di Francesco, S. Grasso, M. Zappalà, Novel peptidomimetics containing a vinyl ester moiety as highly potent and selective falcipain-2 inhibitors, J. Med. Chem. 52 (2009) 2157–2160.
[8] (a) R. Ettari, M. Zappalà, N. Micale, T. Schirmeister, C. Gelhaus, M. Leippe, A. Evers, S. Grasso, Synthesis of novel peptidomimetics as inhibitors of protozoan cysteine proteases falcipain-2 and rhodesain, Eur. J. Med. Chem. 45 (2010) 3228–3233;
(b) F. Bova, R. Ettari, N. Micale, C. Carnovale, T. Schirmeister, C. Gelhaus, M. Leippe, S. Grasso, M. Zappalà, Constrained peptidomimetics as antiplasmodial falcipain-2 inhibitors, BMC 18 (2010) 4928–4938;
(c) R. Ettari, M. Zappalà, N. Micale, G. Grazioso, S. Giofrè, T. Schirmeister, S. Grasso, Peptidomimetics containing a vinyl ketone warhead as falcipain-2 inhibitors, Eur. J. Med. Chem. 46 (2011) 2058–2065.
[9] (a) G. Grazioso, L. Legnani, L. Toma, R. Ettari, N. Micale, C. De Micheli, Mechanism of falcipain-2 inhibition by α,β-unsaturated benzo[1,4]diazepin-2-one methyl ester, J. Comput. Aided Mol. Des. 26 (2012) 1035–1043;
(b) R. Ettari, L. Tamborini, I.C. Angelo, S. Grasso, T. Schirmeister, L. Lo Presti, C. De Micheli, A. Pinto, P. Conti, Development of novel inhibitors of rhodesain with a 3-bromo-isoxazoline warhead, ChemMedChem 8 (2013) 2070–2076;
(c) R. Ettari, N. Micale, G. Grazioso, F. Bova, T. Schirmeister, S. Grasso, M. Zappalà, Synthesis and molecular modeling studies on derivatives of a highly potent peptidomimetic vinyl ester as falcipain-2 inhibitor, ChemMedChem 7 (2012) 1594–1600.
[10] R. Ettari, C. Bonaccorso, N. Micale, C. Heindl, T. Schirmeister, M.L. Calabrò, S. Grasso, M. Zappalà, Development of novel peptidomimetics containing a vinyl sulfone moiety as proteasome inhibitors, ChemMedChem 6 (2011) 1228–1237.
[11] N. Micale, R. Ettari, A. Lavecchia, C. Di Giovanni, K. Scarbaci, V. Troiano, S. Grasso, E. Novellino, T. Schirmeister, M. Zappalà, Development of peptidomimetic boronates as proteasome inhibitors, Eur. J. Med. Chem. 64 (2013) 23–34.
[12] M. Groll, C.R. Berkers, H.L. Ploegh, H. Ovaa, Crystal structure of the boronic acid-based proteasome inhibitor bortezomib in complex with the yeast 20S proteasome, Structure 14 (2006) 451–456.
[13] Y. Zhu, X. Zhu, G. Wu, Y. Ma, Y. Li, X. Zhao, Y. Yuan, J. Yang, S. Yu, F. Shao, R. Li, Y. Ke, A. Lu, Z. Liu, L. Zhang, Synthesis, in vitro and in vivo biological evaluation, docking studies, and structure-activity relationship (SAR) discussion of dipeptidyl boronic acid proteasome inhibitors composed of β-amino acids, J. Med. Chem. 53 (2010) 1990–1999.
[14] (a) R. Ettari, F. Bova, M. Zappalà, S. Grasso, N. Micale, Falcipain-2 inhibitors, Med. Res. Rev. 30 (2010) 136–167;
(b) R. Ettari, L. Tamborini, I.C. Angelo, N. Micale, A. Pinto, C. De Micheli, P. Conti, Inhibition of rhodesain as a novel therapeutic modality for human African trypanosomiasis, J. Med. Chem. 56 (2013) 5637–5658;
(c) N. Micale, R. Ettari, T. Schirmeister, A. Evers, C. Gelhaus, M. Leippe, M. Zappalà, S. Grasso, Novel 2*H*-isoquinolin-3-ones as antiplasmodial falcipain-2 inhibitors, BMC 17 (2009) 6505–6511.
[15] D.S. Matteson, P.K. Jesthi, K.M. Sadhu, Synthesis and properties of pinandiol α-amino boronic esters, Organometallics 3 (1984) 1284–1288.
[16] M. Britton, M.M. Lucas, S.L. Downey, M. Screen, A.A. Pletnev, M. Verdoes, R.A. Tokhunts, O. Amir, A.L. Goddard, P.M. Pelphrey, D.L. Wright, H.S. Overkleeft, A.F. Kisselev, Selective inhibitor of proteasome's caspase-like sites sensitises cells to specific inhibition of the chymotrypsin-like sites, Chem. Biol. 16 (2009) 1278–1289.
[17] A.F. Kisselev, A. Callard, A.L. Goldberg, Importance of different active sites in protein breakdown by 26S proteasomes and the efficacy of proteasome inhibitors varies with the protein substrate, J. Biol. Chem. 281 (2006) 8582–8590.
[18] F. Parlati, S.J. Lee, M. Aujay, E. Suzuki, K. Levitsky, J.B. Lorens, D.R. Micklem, P. Ruurs, C. Sylvain, Y. Lu, K.D. Shenk, M.K. Bennet, Carfilzomib can induce tumor cell death through selective inhibition of the chymotrypsin-like activity of the proteasome, Blood 114 (2009) 3439–3447.
[19] K. Scarbaci, V. Troiano, N. Micale, R. Ettari, L. Tamborini, C. Di Giovanni, C. Cerchia, S. Grasso, E. Novellino, T. Schirmeister, A. Lavecchia, M. Zappalà, Identification of a new series of amides as non-covalent proteasome inhibitors, Eur. J. Med. Chem. 76 (2014) 1–9.
[20] K. Scarbaci, V. Troiano, R. Ettari, A. Pinto, N. Micale, C. Di Giovanni, C. Cerchia, E. Novellino, A. Lavecchia, T. Schirmeister, M. Zappalà, S. Grasso, Development of novel pseudopeptides selective peptidomimetics, containing a boronic acid moiety, targeting the 20S proteasome as anticancer agents, Chem. Med. Chem. (2014), http://dx.doi.org/10.1002/cmdc.201402075.
[21] a) F. Cozzi, M. Cinquini, R. Annunziata, T. Dwyer, J.S. Siegel, Polar/π interactions between stacked aryls in 1,8-diarylnaphthalenes, J. Am. Chem. Soc. 114 (1992) 5729–5733;

b) B.W. Gung, X. Xue, Y. Zou, Enthalpy (ΔH) and entropy (ΔS) for π-stacking interactions in near-sandwich configurations: relative importance of electrostatic, dispersive, and charge-transfer effects, J. Org. Chem. 72 (2007) 2469–2475.

[22] H.D.H. Showalter, Ready access to 7,8-dihydro- and 1,2,3,4-tetrahydro-1,6-naphthyridine-5(6H)-ones from simple pyridine precursors, J. Heterocycl. Chem. 43 (2006) 1311–1317.

[23] Maestro, Version 9.7, Schrödinger, LLC, New York, NY, 2014.

[24] C.C. Huang, G.S. Couch, E.F. Pettersen, T.E. Ferrin, Chimera: an extensible molecular modelling application constructed using standard components, Pacif. Symp. Biocomput. 1 (1996) 724. http://www.cgl.ucsf.edu/chimera.

[25] (a) GOLD, Version 5.2, CCDC Software Limited, Cambridge, U.K., 2008;
(b) G. Jones, P. Willett, R.C. Glen, A.R. Leach, R. Taylor, Development and validation of a genetic algorithm for flexible docking, J. Mol. Biol. 267 (1997) 727–748.

[26] W.L. DeLano, The PyMOL Molecular Graphics System, DeLano Scientific LLC, San Carlos, CA, USA, http://www.pymol.org/.

[27] M.L. Verdonk, G. Chessari, J.C. Cole, M.J. Hartshorn, C.W. Murray, J.W.M. Nissink, R.D. Taylor, R. Taylor, Modeling water molecules in protein-ligand docking using GOLD, J. Med. Chem. 48 (2005) 6504–6515.

[28] M.L. Verdonk, J.C. Cole, M.J. Hartshorn, C.W. Murray, R.D. Taylor, Improved protein-ligand docking using GOLD, Proteins 52 (2003) 609–623.

[29] a) G. Fracchiolla, A. Laghezza, L. Piemontese, P. Tortorella, F. Mazza, R. Montanari, G. Pochetti, A. Lavecchia, E. Novellino, S. Pierno, D. Conte Camerino, F. Loiodice, New 2-aryloxy-3-phenyl-propanoic acids as PPAR α/γ dual agonists with improved potency and reduced adverse effect on skeletal muscle function, J. Med. Chem. 52 (2009) 6382–6393;
b) L. Porcelli, F. Gilardi, A. Laghezza, L. Piemontese, N. Mitro, A. Azzariti, F. Altieri, L. Cervoni, G. Fracchiolla, M. Giudici, U. Guerrini, A. Lavecchia, R. Montanari, C. Di Giovanni, A. Paradiso, G. Pochetti, G.M. Simone, P. Tortorella, M. Crestani, F. Loiodice, Synthesis, characterization and biological evaluation of ureidofibrate-like derivatives endowed with peroxisome proliferator-activated receptor activity, J. Med. Chem. 55 (2012) 37–54;
c) M.G. Perrone, P. Vitale, P. Malerba, A. Altomare, A. Lavecchia, R. Montanari, C. Di Giovanni, E. Novellino, A. Scilimati, Core ring nature in diarylheterocycle COX-1 inhibitors, Chem. Med. Chem. 7 (2012) 629–641;
d) P.M.G. Vitale, Perrone, P. Malerba, A. Lavecchia, A. Scilimati, Selective COX-1 inhibition as a target of novel theranostic diarylisoxazoles, Eur. J. Med. Chem. 74 (2014) 606–618.